

Analogue models of caldera collapse in strike-slip tectonic regimes

Eoghan P. Holohan · Benjamin van Wyk de Vries ·
Valentin R. Troll

Received: 4 August 2005 / Accepted: 18 June 2007 / Published online: 2 September 2007
© Springer-Verlag 2007

Abstract Regional-scale faulting, particularly in strike-slip tectonic regimes, is a relatively poorly constrained factor in the formation of caldera volcanoes. To examine interactions between structures associated with regional-tectonic strike-slip deformation and volcano-tectonic caldera subsidence, we made scaled analogue models. Tabular (sill-like) inclusions of creamed honey in a sand/gypsum mix replicated shallow-level granitic magma chambers in the brittle upper crust. Lateral motion of a base plate sited below half the sand/gypsum pack allowed simulation of regional strike-slip deformation. Our experiments modelled: (1) strike-slip deformation of a homogeneous brittle medium; (2) strike-slip deformation of a brittle medium containing a passive magma reservoir; (3) caldera collapse into sill-like magma reservoirs without regional strike-slip deformation; and (4) caldera collapse into sill-like magma reservoirs after regional strike-slip deformation. Our results show that whilst the magma chamber shape principally influences the development and geometry of volcano-tectonic collapse structures, regional-tectonic strike-slip faults (Riedel shears and Y-shears) may affect a caldera's structural evolution in two main ways. Firstly, regional

strike-slip faults above the magma chamber may form a pre-collapse structural grain that is exploited and reactivated during subsidence. Our experiments show that such faults may preferentially reactivate where tangential to the collapse area and coincident with the chamber margins. In this case, volcano-tectonic extension in the caldera periphery tends to localise on regional-tectonic faults that lie just outside the chamber margins. In addition, volcano-tectonic reverse faults may link with and reactivate pre-collapse regional-tectonic faults that lie just inside the chamber margins. Secondly, where regional-tectonic strike-slip faults define corners in the magma chamber margin, they may halt the propagation of volcano-tectonic reverse faults. The experiments also highlight the potential difficulties in assessing the relative contributions of volcano-tectonic and regional-tectonic subsidence processes to the final caldera structure seen in the field. Disruption of the pre-collapse surface by regional-tectonic faulting was preserved during coherent volcano-tectonic subsidence to produce a caldera floor of differentially-subsided fault blocks. Without definitive evidence for syn-eruptive growth faulting, thickness changes in caldera fill across such regional-tectonic fault blocks in nature could be mistaken as evidence for piecemeal volcano-tectonic collapse.

Editorial responsibility: J Stix

E. P. Holohan (✉) · V. R. Troll
Department of Geology, School of Natural Sciences,
Trinity College,
Dublin 2, Ireland
e-mail: holohane@tcd.ie

B. van Wyk de Vries
Laboratoire Magmas et Volcans,
5 rue Kessler,
63038 Clermont-Ferrand, France
e-mail: B.vanwyk@opgc.univ-bpclermont.fr

Keywords Caldera volcanoes · Subsidence ·
Volcano-tectonics · Strike-slip tectonics · Analogue models

Introduction

The voluminous eruptions associated with catastrophic caldera formation (e.g. Krakatau in 1883 and Tambora in 1815—Self et al. 1984) can devastate vast areas and perhaps alter global climate (Rampino and Self 1992). Generally

considered to form through collapse of a magma chamber roof of diameter >1 km, calderas thus constitute a major geohazard. Precisely why and how this collapse process occurs remains unclear, however (see reviews of Lipman 1997; Cole et al. 2005). Violent syn-collapse eruptions preclude direct observation, and collapse-related structures are generally ill-exposed, especially at geologically young and/or ‘restless’ calderas. Here, collapse structures usually lie buried beneath a 0.1–3 km thick infill of syn-collapse ash-flow deposits (ignimbrites) and other sediments, as well as post-collapse lakes and lavas. Some ancient, deeply-eroded calderas display lower structural levels including the caldera floor (subsided pre-collapse surface), but post-collapse deformation and intrusions commonly overprint or obliterate the subsidence phase structures. Also, linkage to the post-collapse surface morphology and upper structural levels seen at younger calderas is uncertain.

Consequently, many studies of subsidence systems analogous to collapse calderas have been conducted (e.g. Komuro 1987; Marti et al. 1994; Branney 1995; Roche et al. 2000; Acocella et al. 2000; Walter and Troll 2001; Troll et al. 2002; Kennedy et al. 2004). These studies conclude that a caldera resulting from magma chamber evacuation and withdrawal of magmatic roof support (cf. Druitt and Sparks 1984) may possess two generalised structural zones (Fig. 1—see also Lipman 1997). The outermost of one or more ring-faults of vertical to outward dip and reverse motion bounds a *central caldera zone*. Central zone subsidence generates a concentric *peripheral caldera zone*, which stretches from the outermost reverse ring-fault to an outermost normal ring-fault of steep inward dip (Fig. 1). This peripheral zone is characterised by crevasse opening, horst and graben formation, inward rotation of strata and structures, and mass movement of rock toward the caldera centre.

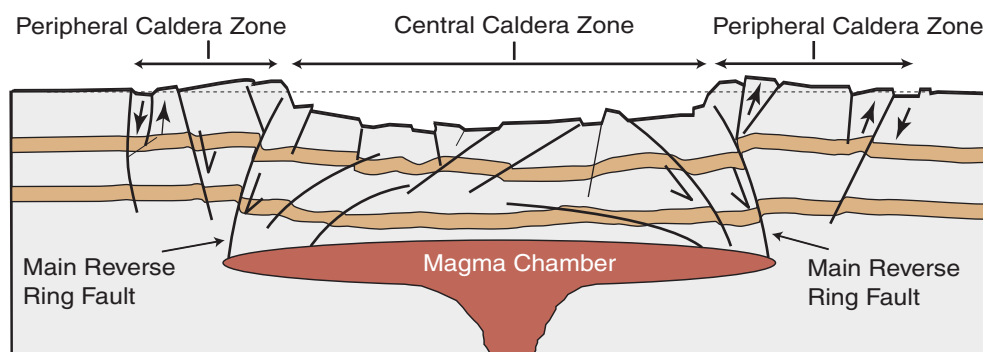
An acknowledged limitation of most previous analogue and numerical studies of caldera formation is the absence of pre-collapse regional faults. Indeed, exceptionally detailed field studies in ancient, well-exposed calderas (e.g. Glencoe, Scotland—Moore and Kokelaar 1998) highlight several potential influences of regional-tectonic structures in caldera

evolution. Investigation of the role(s) of regional-tectonic setting and structures in caldera development remains at an embryonic stage (cf. Lipman 1997; Cole et al. 2005), however. A symptom of this is the ambiguity around the term ‘volcano-tectonic’. This term has variously described structures or structural depressions that are: (a) generated solely by regional-tectonic processes, but host volcanic deposits (Lipman 1997 and references therein); (b) generated by regional-tectonic processes, but with some displacement related to magmatic/volcanic activity (Nappi et al. 1991); and (c) generated solely by magmatic/volcanic activity (Branney and Kokelaar 1994). In this paper, ‘volcano-tectonic’ refers to faults or fault motions generated by local magmatic/volcanic processes only. Likewise, ‘regional-tectonic’ refers to faults or fault motions generated by regional-scale deformation processes.

Building on Acocella et al. (2004) and Holohan et al. (2005), we studied how regional-tectonic faults might affect caldera formation by constructing scaled analogue models, but we focus on the case of regional strike-slip systems. Regional-tectonic settings with active strike-slip deformation and young or ‘restless’ calderas include:

1. *Oblique rifts* of varied transtensive components, e.g. Taupo Volcanic Zone—Rotorua and Kapenga calderas (Spinks et al. 2005); Ethiopian Rift—Fantale and Gedemsa calderas (Acocella et al. 2003)
2. *Transfer zones* between segments of orthogonal or oblique rifts, e.g. Rio Grande Rift—Valles caldera (Goff and Gardner 1994); Phlegrean Volcanic District—Campi Flegrei caldera (Acocella et al. 1999); East African Rift—Suswa and Longonot calderas (Skilling 1993)
3. *Major shear zones*, along which calderas may form either in zones of diffuse lateral shear, e.g. Olacapato – El Toro fault zone – Negra Muerta caldera (Riller et al. 2001) or in pull-apart graben at releasing bends or relay zones, e.g. Great Sumatran Fault Zone—Toba and Ranau calderas (Bellier and Sebrier 1994), Nicaraguan depression—Masaya caldera (Girard and van Wyk de Vries 2005)

Fig. 1 Sketch of structures generated during simulated magma chamber evacuation (balloon deflation) and caldera collapse (adapted from Walter and Troll 2001)



Volcano-tectonic reactivation of regional-tectonic strike-slip faults is thought to have profoundly influenced the development and geometry of many of these calderas, which include some of the world's largest and most active—e.g. Toba caldera (Aldiss and Ghazali 1984; Bellier and Sebrier 1994) and Campi Flegrei caldera (Orsi et al. 1996). One possible influence of strike-slip faults on the formation of such calderas is to provide a structural grain to be exploited during subsidence, as inferred at Glencoe caldera (Moore and Kokelaar 1998). Another possible influence of strike-slip faults is to define the pre-collapse magma chamber (granitic pluton) boundaries. Field (e.g. Hutton and Reavy 1992), theoretical (e.g. Bosworth et al. 2003) and experimental (e.g. Roman-Berdiel 1999) studies conclude that regional-tectonic structures and stress fields strongly affect pluton geometry during and after emplacement. Resultant pre-caldera plutons are predominantly elongate in plan-view, and commonly have some fault-controlled boundaries (e.g. Cruden 1998). Although the strong control of magma chamber geometry on subsequent caldera geometry is experimentally well-established (e.g. Roche et al. 2000), most previous analogue and numerical caldera studies assumed a perfectly circular plan view chamber shape. Considering therefore the case of elongate magma chamber deflation in strike-slip to transtensional regimes, we show that regional-tectonic structures can indeed influence caldera development through a combination of structural grain exploitation and magma chamber boundary control.

Experiment design and scaling

Model construction

For rock at shallow crustal levels, we used fine-grained (0.09–0.25 mm diameter), well-sorted sand mixed at 4:1 by volume with gypsum powder (cf. Donnadieu and Merle 1998; Girard and van Wyk de Vries 2005). As our analysis focussed on high-level deformation above the brittle–ductile transition in the Earth's upper crust, a ductile lower crust component was excluded from our models. To simulate granitic magma, we used creamed honey, which has a surface tension and viscosity high enough to retard significant permeation into the sand. We conducted four experiment series to establish: (1) structures due to regional strike-slip deformation; (2) how a passive (i.e. neither inflating nor deflating) magma chamber might affect these regional strike-slip structures *prior* to caldera collapse; (3) structures due to caldera collapse into circular and elliptical magma chambers; and (4) how caldera collapse structures develop after regional strike-slip faulting of the magma chamber roof and environs.

Regional strike-slip control experiments (Con 1–8, Con B1–B2)

On a fixed table lay a 5.5 cm thick sand–gypsum pack, under one half of which was a thin, rigid basal plate (Fig. 2a, b). Computer-controlled motion of the basal plate generated a velocity discontinuity, and consequently a shear zone, within the sand pack. Dextral strike-slip motion was arbitrarily imposed in all experiments with regional shear. The 'opening angle' between the base plate's long edge and its horizontal motion vector determined the component of dilation accompanying shear along the velocity discontinuity (cf. Girard and van Wyk de Vries 2005), and was varied between experiments (Tables 2 and 3). Parallel marker lines on the sand surface (e.g. Fig. 3) helped track lateral offsets.

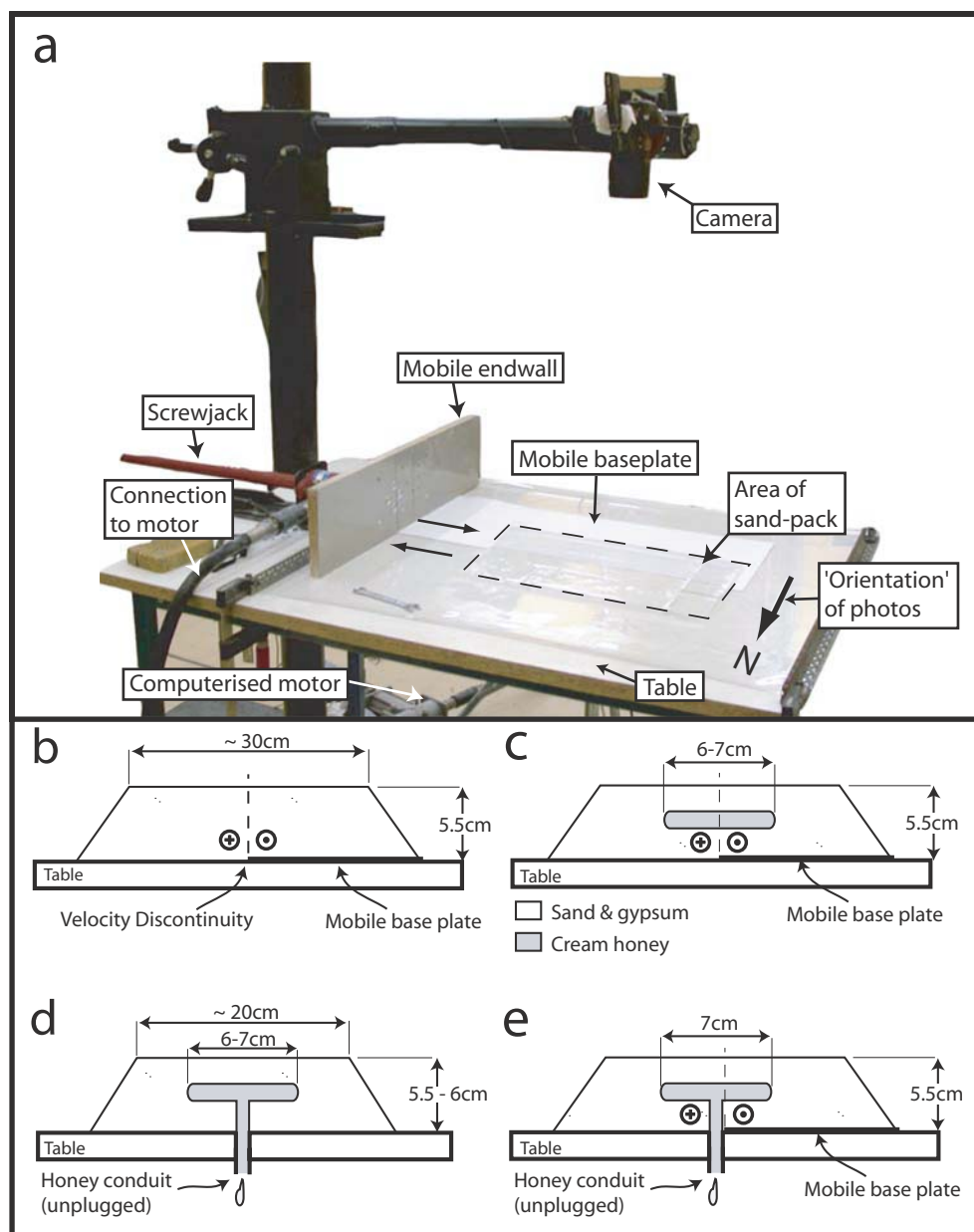
Regional strike-slip with passive magma chamber experiments (Mag 1–22, Mag B1–B8)

The set-up here (Fig. 2c) matched that described above, but with the inclusion in the sand pile of a honey chamber of laccolithic or tabular geometry (thought to be the most common form for natural granitic plutons—Cruden 1998). The sand pile was initially levelled off at the desired depth of the honey chamber base. A cylindrical mould was placed on the sand surface and filled with honey to the scaled chamber thickness (1–2.5 cm). The sand pile was then built up around the mould to the honey level, and the mould was slowly extracted. After sufficient time elapsed to ensure a flat honey surface (no wrinkles or ridges), sand was carefully and evenly placed over the chamber to make the roof. The sand-pile was then levelled off at a total height of 5.5 cm. If any roof subsidence occurred during this procedure, the experiment was aborted. Chambers were initially circular and 7 cm in plan view diameter, except for three slightly elliptical chambers (7×6 cm) with long axes parallel to the velocity discontinuity. The thickness of the honey lozenge, the distance from its centre to the velocity discontinuity, and its depth in the sand pile were varied (Table 2b).

Caldera collapse control experiments (Cal Stat 1–7)

To construct a conduit for honey evacuation (Fig. 2d), a vertical hole of 1 cm diameter was first drilled through the table and lined with a pipe of 1 mm wall thickness. The pipe was plugged at its lower end and a honey-filled syringe was fixed upright in its upper end. The sand pile was then levelled off around the syringe at a height corresponding to the desired depth of the chamber base. To fill the pipe and link it to the chamber base, the syringe was withdrawn upward to the levelled sand surface, while simultaneously squeezing out more honey. The honey chamber was then emplaced into the sand-pack as described

Fig. 2 **a** Photo of experimental apparatus for strike-slip deformation. Cross-section sketches of experimental configurations for: **b** strike-slip deformation in purely brittle crust; **c** strike-slip deformation of brittle crust containing a passive magma chamber; **d** caldera collapse without regional faulting; and **e** caldera collapse following regional strike-slip faulting



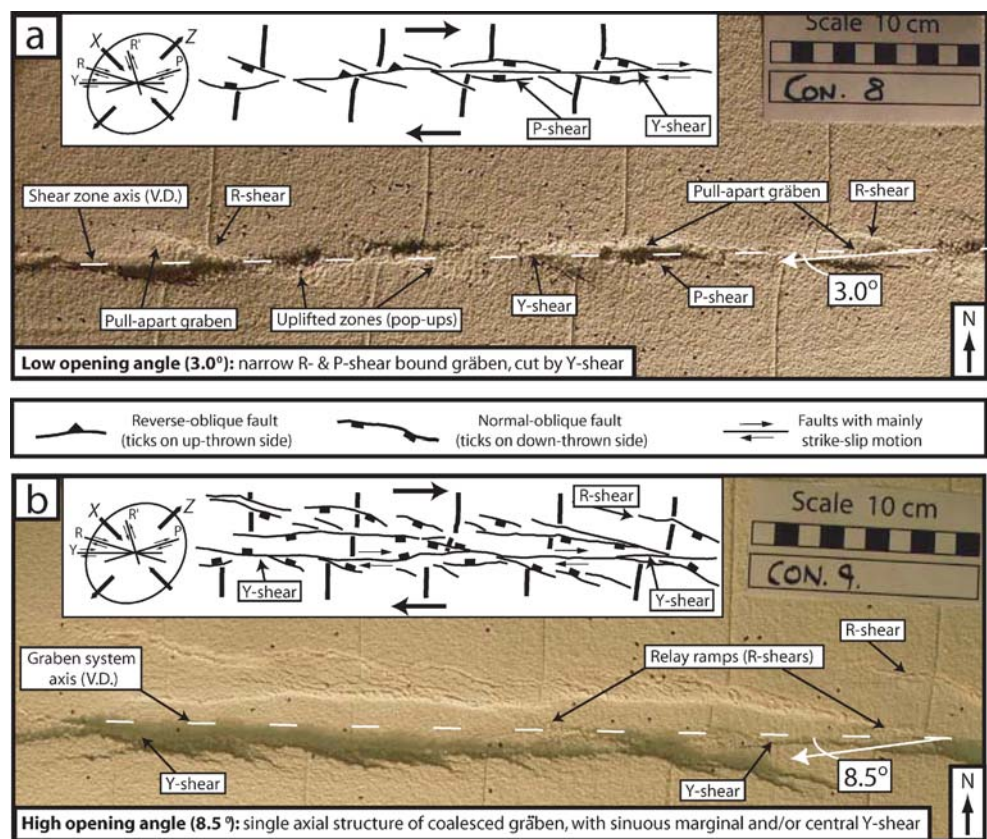
above. Unplugging the lower end of the pipe caused evacuation of the honey chamber via the conduit, destabilisation of the roof, and onset of caldera collapse. Although collapse was thus in response to fluid outflow, rather than vice versa (see Roche et al. 2000), resultant structures closely matched those of past analogue studies (e.g. Roche et al. 2000; Kennedy et al. 2004), and so any deformation imposed by fluid flow was negligible.

Syn- to post-tectonic caldera collapse experiments (*Cal Mag 1–19*)

Construction of all components in this set-up (Fig. 2e) is described above. All chambers were initially circular, 7 cm

in diameter, and centred on the conduit. Chamber depth, thickness, and distance from the velocity discontinuity to the chamber centre were varied (Table 3b). Transtensive regional motion was imposed on the sand pile at the same velocity as for the passive chamber experiments. After around 1.7 cm of regional strike-slip displacement, the conduit was unplugged to initiate caldera collapse and basal plate motion was reduced to the slowest speed possible (0.03 cm h^{-1}), or stopped (most cases). This caused 0–2 mm of regional-tectonic fault movement (0–400 m in nature according to the scaling below) during collapse. Experiments run with and without syn-collapse regional-tectonic displacement showed essentially the same outcomes, however.

Fig. 3 Simulation of strike-slip deformation in brittle crust (light from S). **a** At low opening angles (3°), a narrow shear zone forms with small, Riedel shear bound, pull-apart-type gräben and occasional pop-ups. **b** At higher opening angles (8.5°), a series of rhombic pull-apart-type gräben forms along a broader shear zone. These gräben rapidly coalesce to form a single graben system. *Insets* show sketches of structures and their theoretical orientation with respect to the incremental strain ellipse (Woodcock and Schubert 1994)



Scaling considerations

Analogue models should obey the principle of similarity (Hubbert 1951), whereby lengths, deformation rates, material properties, and forces in experiment should scale to those in nature. A scaling ratio for any given physical property is $X^* = X_{\text{Model}}/X_{\text{Nature}}$ and relates to scaling ratios for other properties through standard physical equations. As the timeframes of pre-collapse regional tectonics and syn-collapse caldera formation differ greatly in nature, they must be scaled as separate deformation phases in experiment (Table 1).

Brittle failure of sand and rock *approximates* a Coulomb criterion defined by the material cohesion and angle of internal friction (Hubbert 1951; Schellart 2000). The length ratio, $l^* = l_{\text{Model}}/l_{\text{Nature}}$ (geometric scaling factor) was 5×10^{-6} , so that 1 cm in the model corresponds to ~ 2 km in nature. The stress and cohesion ratio, $\sigma^* = \sigma_{\text{Model}}/\sigma_{\text{Nature}}$ (dynamic scaling factor) is calculated from the equation $\sigma^* = \rho^* g^* l^*$. The angle of internal friction of the sand/gypsum mix ($\phi_{\text{SG}} \sim 37^\circ$ from maximum sand/gypsum cone slope) matches that of natural rocks ($\phi_{\text{Nature}} = 30 - 45^\circ$ —Goodman 1989). The sand/gypsum mixture's density was around 1400 kg m^{-3} , whereas that of most natural rock types (granites, basalts, hard limestones, etc.) lies between $2,600 - 3,000 \text{ kg m}^{-3}$ (Goodman 1989). As the analogue material density is half that of natural rocks (i.e. $\rho^* = 0.5$)

and gravitational acceleration is the same in both model and nature (i.e. $g^* = 1$), the required stress ratio for a geometric scaling factor of 5×10^{-6} is $\sigma^* = 2.5 \times 10^{-6}$. Cohesion of natural rocks lies in the range of $10^5 - 10^8 \text{ Pa}$ (Schellart 2000 and references therein), although mechanical anisotropies (fractures, etc.) will result in cohesions less than the range maximum—perhaps around 10^6 Pa (Schultz 1996). When the above natural cohesion range is scaled down by 2.5×10^{-6} , the required analogue material cohesion is $0.25 - 250 \text{ Pa}$. At normal stresses applied in the models, cohesion of dry, fine-grained sand is $0 - 250 \text{ Pa}$ (Schellart 2000); addition of finer material like gypsum or flour raises this value only slightly (e.g. $\sigma_{\text{Model}} \approx 200 \text{ Pa}$ in Donnadieu and Merle 1998). Scaling of brittle material behaviour is theoretically time-independent, and is thus the same for the regional and caldera deformation phases.

Scaling of ductile behaviour is time-dependent, however, as viscosity (η) ratios relate to stress (σ^*) and time (T^*) ratios through the equation $\eta^* = \sigma^* T^*$. The time ratio $T^* = l^*/V^*$, where V is velocity. For the regional deformation phase, slip rates along major strike-slip faults can exceed 2.5 cm y^{-1} (e.g. the Great Sumatran Fault—Bellier et al. 1999), which for a model strike-slip rate of 1 cm h^{-1} gives velocity and time ratios of $V_r^* = 3.5 \times 10^3$ and $T_r^* = 1.4 \times 10^{-9}$. Durations of 1.5–4 h typical for the model regional deformation phase (Tables 2 and 3) thus

Table 1 Outline of scaling adopted for two deformation phases, regional-tectonic strike-slip and volcano-tectonic caldera subsidence. Values of parameters in model and nature are also given

Physical properties	Deformation phase 1: regional strike-slip	Deformation phase 2: caldera collapse
Length (l), density (ρ), gravity (g), & stress/cohesion (σ) (geometric & dynamic similarity)	$l^* = l_m/l_n = 5 \times 10^{-6}$; $\rho^* = \rho_m/\rho_n = 0.5$; $g^* = g_m/g_n = 1$ $\sigma^* = \rho^* g^* l^* = (0.5)(1)(5 \times 10^{-6}) = 2.5 \times 10^{-6} = \sigma_m/\sigma_n$ \Rightarrow If $\sigma_n = 10^5 - 10^8 \text{ Pa}$, $\sigma_m = 0.25 - 250 \text{ Pa}$	As for phase 1 As for phase 1
Velocity (V) & time (T) (kinematic similarity)	$V^* = V_m/V_{nr} = 3.5 \times 10^3$ $T_r^* = l^*/V_r^* = (5 \times 10^{-6})/(3.5 \times 10^3) = 1.4 \times 10^{-9} = T_m/T_n$ \Rightarrow If $T_{nr} = 5.4 \times 10^3 - 1.4 \times 10^4 \text{ s}$, $T_{nr} = 3.9 \times 10^{12} - 1 \times 10^{13} \text{ s}$	$V_c^* = V_{mc}/V_{nc} = 3.2 \times 10^{-5}$ $T_c^* = l^*/V_c^* = (5 \times 10^{-6})/(3.2 \times 10^{-5}) = 1.5 \times 10^{-1}$
Viscosity (η)	$\eta_r^* = \sigma^* T_r^* = (2.5 \times 10^{-6})(1.4 \times 10^{-9}) = 3.5 \times 10^{-15} = \eta_m/\eta_n$ \Rightarrow If $\eta_{nr} = 200 - 600 \text{ Pas}$, $\eta_{nr} = 5.7 \times 10^{16} - 1.7 \times 10^{17} - \text{Pas}$	$\eta_c^* = \sigma^* T_c^* = (2.5 \times 10^{-6})(1.5 \times 10^{-1}) = 3.9 \times 10^{-7} = \eta_m/\eta_n$ \Rightarrow If $\eta_{nc} = 200 - 600 \text{ Pas}$, $\eta_{nc} = 5.1 \times 10^8 - 1.5 \times 10^9 \text{ Pas}$
Model parameters	Natural parameters Length (l_n) = 2 km = $2 \times 10^3 \text{ m}$ Density of sand + gypsum (ρ_n) = 2600 – 3000 kg m $^{-3}$ Gravity (g_n) = 9.8 m s $^{-2}$ Cohesion of crustal rocks (ρ_n) = $10^5 - 10^8 \text{ Pa}$ Angle of internal friction (α_n) = 30 – 45 $^\circ$ Strike-slip velocity (V_{nr}) = 2.5 cm year $^{-1}$ = $7.9 \times 10^{-10} \text{ m s}^{-1}$ Chamber residence time (T_{nr}) = 1.5 – 4 h = $5.4 \times 10^3 - 1.4 \times 10^4 \text{ s}$ Caldera-collapse velocity (V_{mc}) = 0.2 cm hr $^{-1}$ = $5.6 \times 10^{-7} \text{ m s}^{-1}$ Viscosity of creamed honey (η_m) = 200 – 600 Pas	References Goodman 1989 Schellart 2000 Goodman 1989 Bellier et al. 1999 Jellinek and DePaolo 2003
Viscosity of creamed honey (η_m) = 200 – 600 Pas	Viscosity of granitic magma (η_n) = $10^4 - 10^{12} \text{ Pas}$	Dingwell 1999

Table 2 Experimental data from control experiments simulating (a) strike-slip deformation in purely brittle crust, and (b) strike-slip deformation of brittle crust containing a passive magma chamber

a) Tectonic Controls									Observations/Remarks	
Expt. No.	Title	Opening Angle (deg.)	Displacement (cm)	Position (cm)	Chamber	Position of chamber				
1	Con B2	2.4	6							
2	Con 8	3	5							
3	Con B1	3.1	4							
4	Con 3	4.5	2.5							
5	Con 6	5.5	2.8							
6	Con 9	8.5	3.7							
7	Con 4	11	2.5							
8	Con 1	14	2.5							

b) Chamber & Tectonic Interaction controls											
Expt. No.	Title	Opening Angle (deg.)	Displacement (cm)	Position (cm)	Chamber	Position of chamber	Position of chamber	Observations/Remarks	Chamber localised graben/faults?	Code	
1	Mag 21	0.7	3	7	7	1.5	1	3.0 N	Pop-ups along shear zone. Subtle depression above chamber, otherwise as controls with low opening angle	No	1
2	Mag 1	2.5	2.3	7	6	1	2.5	1.5 N	Small graben in shear zone. Intrusion or dragging of honey down the main shear zone (Y-shear), otherwise as controls with low opening angle	No	1
3	Mag 2	2.5	2.8	6	6	1	2.5	1.0 S	Sinistral regional shear imposed, not dextral. Small graben along shear zone, except above chamber.	No	1
4	Mag 22	2.5	3	7	7	1.5	1	3.0 S	No graben along shear zone, only pop-ups, as controls with low opening angle.	No	1
5	Mag Cal 6	2.9	1.5	7	7	1.5	1.5	2.0 N	Pop-ups and narrow pull-apart graben along shear zone, as controls with low opening angle.	No	1
6	Mag 17	3.2	2.8	6.5	6.5	1	1	0.75 N	Graben in shear zone to W, pop-ups to E. Intrusion of honey down the main Y-shear. At chamber have sigmoidal bulge & shear zone widens.	Yes (to N & S, weak)	2
7	Mag 19	3.2	2.8	7	6.5	1	1	2.5 S	Narrow graben along shear zone to E and W of chamber. Above chamber along shear zone, have pop-ups	Yes (to S, weak)	2
8	Mag 20	3.3	3	7	7	1	1	3.0 N	Graben to W, graben to E. Pop-ups where chamber intersects shear zone. V. subtle depression above chamber & curved fault along NE rim.	Yes (to N, v. weak)	2
9	Mag B2	3.3	4	7	7	1	1	0	Segmented axial graben system forms. Big bulge above chamber toward experiment end.	No	1
10	Mag 7	3.5	2.5	6.5	6.5	1.3	1.7	0	Initially pop-ups in E of shear zone, then narrow graben all along shear zone.	Yes (to S, subtle)	2
11	Mag 18	3.5	2.8	7	7	1	1	0	Graben in W of shear zone, but narrow. None to E. Sigmoidal bulge above chamber & shear zone widens to 7.5 cm here.	Yes (to N & S, weak)	2
12	Mag B1	4	7	7	7	1.5	1.5	0	Ran to & measurements at 7.5 cm reg. displ. Minimal subsidence above chamber centre.	Yes (v. good to S, subtle N)	3
13	Mag B5	4	3.5	7	7	1	3	0	Restricted subsidence over chamber. Narrow graben to E and W along shear zone. Honey intrusion down Y-shear.	Maybe (to S)	2
14	Mag B8	4	6	7	7	1	2	3.0 S	Narrow graben system and Riedels formed. Deformation of chamber limited to edge next to shear zone (V.D.).	Yes (to S, v. good)	3
15	Mag B7	4.3	2.8	7	7	1	2	1.0 N	Restricted subsidence and even bulging over chamber. Narrow graben to E and W. Anti-Riedel shears preserved as cracks in graben floors.	Yes (subtle to N)	2
16	Mag B4	4.5	5	7	7	1	2	0	En-echelon graben delimited by Riedel shears merge to form axial graben system. Restricted subsidence over chamber centre.	Yes (to N & S, v. good)	3
17	Mag Cal 5	4.5	1.7	7	7	1.5	2.5	1.0 N	Narrow graben along shear zone E and W of chamber. Restricted subsidence above chamber.	Yes (to N, weak)	2
18	Mag B3	5	3.8	7	7	1	1.5	0	Axial graben system along shear zone E & W of chamber. Restricted subsidence over chamber centre. Anti-Riedel fractures preserved in graben.	Yes (to N & S, v. good)	3
19	Mag Cal 12	5	1.7	7	7	1	3	2.0 N	En-echelon graben delimited by Riedel shears along shear zone to E and W of chamber. Restricted subsidence over chamber centre.	Yes (to N, weak)	2
20	Mag Cal 11	5.7	1.5	7	7	1.5	1.5	2.0 N	En-echelon graben delimited by Riedel shears along shear zone to E and W of chamber. Restricted subsidence over chamber centre.	Yes (to N, v. good, & S)	3
21	Mag Cal 1	6	1	7	7	2	1	1.0 N	Riedel shear bound graben to W. Otherwise limited subsidence along shear zone.	Yes (to N, weak)	2
22	Mag Cal 3	6	1.7	7	7	1.5	1.5	1.5 N	Narrow graben systems bound by Riedel shears and P-shears all along shear zone. Slightly less subsidence above chamber.	Yes (to N, weak)	2
23	Mag Cal 4	6	1.8	7	7	1	3	0.75 N	En-echelon graben delimited by Riedel shears along shear zone to E and W of chamber. Restricted subsidence over chamber centre.	Yes (to S, v. good)	3
24	Mag Cal 2	6.3	1.5	7	7	1	2	1.0 N	En-echelon Riedel shears along shear zone to W. Riedel-bound graben to E of chamber. Restricted subsidence generally though.	Yes (to N, weak)	2
25	Mag B8	7.5	3.2	7	7	1	2	1.0 S	Axial graben system, partially segmented with Riedel-shear relay ramps. Restricted subsidence over chamber. Honey intrusion down Y-shear.	Yes (to S, v. good, subtle N)	3
26	Mag 11	7	2.7	7	7	1	2	2.5 S	Riedel and Y-shear bound graben along shear zone, but narrower and shallower to E. Very little subsidence where chamber edge meets shear zone.	Yes (to S, v. subtle)	2
27	Mag 3	-8	2.6	6	6	1	2	0.5 S	Axial graben system, partially segmented, Riedel-shear relay ramps. Subsidence over chamber same as shear zone. Chamber cut by two Y-shears.	Yes (to N & S, v. good)	3
28	Mag Cal 7	8	4	7	7	1.5	1.5	2.0 N	Narrow axial graben forms. Unusual structure. Better developed along E and W of shear zone, less so in centre near chamber.	Yes (to N, v. good, & S)	3
29	Mag 5	9	2.7	6	6	1	2	0	Axial graben system, segmented with Riedel-shear relay ramps in E. Subsidence over chamber slightly less than elsewhere along shear zone.	Yes (to S, v. good, subtle N)	3
30	Mag 13	9	2.7	7	7	1.2	1.8	3.5 S	Axial graben system, segmented with Riedel-shear relay ramps in E. Shear zone widens across chamber.	Yes (to S, later overprinted)	2
31	Mag 9	11	2.5	7	6.5	1.5	1.5	2.5 S	Axial graben system, segmented with Riedel-shear relay ramps in E. Shear zone widens across chamber. Subsidence over chamber less.	Yes (to S, v. good)	3

* in cm south or north of the velocity discontinuity between baseplate and table

E = East, W = West, N = North, S = South; V.D. = velocity discontinuity between baseplate and table. Code for graben development: 1 = Poor, 2 = Clear, 3 = Very Clear

scale to $1.2\text{--}3.2 \times 10^5$ years in nature. This range is within that of $10^5\text{--}10^6$ years, over which large caldera-forming magmatic centres are believed to accumulate and reside in the Earth's crust (Jellinek and DePaolo 2003).

Measured before each experiment with a rotary viscometer, creamed honey viscosity was $\sim 200\text{--}600$ Pa s, which through the viscosity equation, scales to $\eta_{nr} = 5.7 \times 10^{16} - 1.7 \times 10^{17}$ Pa.s for the regional deformation phase. Depending on temperature and water content, experimentally derived viscosities for granitic melts range from $10^4\text{--}10^{12}$ Pa s (Dingwell 1999). As cooling, degassing, and crystallisation occur, however, viscosities in assembling granite plutons possibly approach values up to 10^{18} Pa s (Scaillet et al. 1997)—particularly around the pluton margins. Past analogue studies of syn-tectonic granite emplacement into strike-slip or transpressive regimes (Benn et al. 1998; Roman-Berdiel 1999; Corti et al. 2005) assume similar or higher natural granite viscosities to those in the regional deformation phase here.

The caldera deformation phase occurs on geologically instantaneous timescales relative to the time-spans of large-scale regional tectonics and batholith construction. Catastrophic collapse over hours to days (e.g. Long Valley caldera—Hildreth and Mahood 1986) can result in subsidence of ~ 100 m to 5 km (e.g. Stillwater caldera complex—John 1995). A natural subsidence rate of ~ 3 km over ~ 48 h, i.e. $V_{nc} = 1.7 \times 10^{-2} \text{ms}^{-1}$, was replicated in our models as 1 cm in 5 h (on average—Table 3), i.e. $V_{mc} = 5.6 \times$

10^{-7}ms^{-1} . This gives $V^* = 3.2 \times 10^{-5}$, which with $l^* = 5 \times 10^{-6}$, yields $T^* = 1.5 \times 10^{-1}$. Through the viscosity equation, the honey thus scales to a natural viscosity of $\eta_{nc} = 5.1 \times 10^8 - 1.5 \times 10^9$ Pa.s for the caldera collapse deformation phase. Such viscosities are at the higher end of the experimentally-defined range for a pure melt, but are lower than the bulk viscosity of a semi-crystallised pluton (Scaillet et al. 1997). They may thus characterise a mobile, eruptible granitic magma fraction that is crystal-rich (20–50% phenocrysts – e.g. the Youngest Toba Tuff – Chesner 1998), and has relatively low temperatures (700–800°C) and water contents (2–3 wt.%). Within the caldera collapse phase, caldera slip rate and regional slip rate must be scaled directly. Since caldera collapse velocity, $V_{nc} = 1.7 \times 10^{-2} \text{ms}^{-1}$ and regional strike-slip velocity, $V_{nr} = 7.9 \times 10^{-10} \text{ms}^{-1}$, natural caldera collapse rate is about 20 million times faster than contemporaneous regional deformation rate. This relationship was replicated in most experiments by switching off the motor (i.e. $V_{mr}=0$) whilst the honey chamber evacuated.

Experimental results

To aid description of results from experiments with tectonic deformation, we use a compass-like directional convention, whereby the moving base plate occupies the ‘southern’ half

Table 3 Experimental data from experiments simulating (a) caldera collapse without regional faulting and (b) caldera collapse following regional strike-slip faulting

a) Caldera collapse controls		Initial conditions				Final conditions				Observations/Remarks				
Expt. No.	Title	Initial plan-view chamber shape	Chamber long axis (cm)	Chamber short axis (cm)	Chamber thickness (cm)	Chamber depth (cm)	Vertical roof aspect ratio*	Central zone long axis (cm)	Central zone short axis (cm)	Central zone aspect ratio	Peripher al zone long axis (cm)	Peripher al zone short axis (cm)	Peripher al zone aspect ratio	
		Circle	6	6	1	0.5	0.08	5.2	5.2	1.00	7.6	7.2	0.95	
1	Cal Stat 1	Circle	6	6	1	0.5	0.08	5.2	5.2	1.00	7.6	7.2	0.95	
2	Cal Stat 2	Circle	7	7	1.5	1.7	0.24	5.2	5.5	0.95	9.2	8.3	0.90	
3	Cal Stat 3	Circle	7	7	1.5	1.5	0.21	4.5	4.5	0.87	8.6	8	0.93	
4	Cal Stat 4	Circle	7	7	1.2	2.3	0.33	4.8	4.8	0.87	8	7.8	0.98	
5	Cal Stat 5	Ellipse	8	7	0.88	2.3	0.29	4	4	0.67	9.8	9	0.92	
6	Cal Stat 6	Ellipse	8.1	6.5	0.80	2.3	0.28	2.4	2.4	0.40	9.5	8.1	0.85	
7	Cal Stat 7	Ellipse	8.5	7	0.82	2.1	0.25	3.7	3.7	0.65	9.7	9.2	0.95	
* Vertical roof aspect ratio for elliptical honey chambers taken as roof thickness/long axis of honey chamber (cf. Roche et al. 2000)														
E = East; W = West; N = North; S = South														
b) Syn- or Post-tectonic Caldera Collapse		Initial conditions				Final conditions				Observations/Remarks				
Expt. No.	Title	Pre-collapse regional displace.	Chamber Long axis (cm)	Chamber short axis (cm)	Chamber thickness (cm)	Chamber depth (cm)	Vertical roof aspect ratio*	Central zone long axis (cm)	Central zone short axis (cm)	Central zone aspect ratio	Peripher al zone long axis (cm)	Peripher al zone short axis (cm)	Peripher al zone aspect ratio	
		1	8.8	6.7	0.76	2	1	0.11	7	3	0.43	10.7	9.5	0.89
1	Mag Cal 1	1	8.8	6.7	0.76	2	1	0.11	7	3	0.43	10.7	9.5	0.89
2	Mag Cal 2	1.5	8.5	6.6	0.78	1	0.24	6.5	3	0.46	10.4	10	0.96	
3	Mag Cal 3	1.7	8.6	6.1	0.71	1.5	0.17	6	2.5	0.42	9.9	9	0.92	
4	Mag Cal 4	1.5	8.6	6.1	0.71	1.5	0.35	6.5	1.8	0.28	11.1	9.3	0.84	
5	Mag Cal 5	1.7	9	6.5	0.72	1.5	0.28	5.5	2.3	0.45	11	8.5	0.86	
6	Mag Cal 6	1.5	9.6	6.5	0.66	1.5	0.16	5	3.4	0.57	9.1	8.8	0.97	
7	Mag Cal 7	4	10	5.7	0.57	1.5	0.15	5	5	1.00	7	6.9	0.89	
8	Mag Cal 10	1.7	8.5	6.7	0.79	1.5	0.16	5.7	3.6	0.63	9.2	8.7	0.95	
9	Mag Cal 11	1.5	8.8	6.5	0.74	1.5	0.17	210	6.2	3.7	9.8	8.2	0.84	
10	Mag Cal 12	1.7	8.5	6.5	0.76	1	0.35	300	5.7	0.60	9.8	8.7	0.89	
11	Mag Cal 14	1.4	9.5	8	0.84	1.5	0.21	50	7.7	0.71	10.7	9	0.84	
12	Mag Cal 16	1.5	9.2	6.8	0.74	1.5	0.22	70	6.6	0.52	9.8	7.3	0.74	
13	Mag Cal 17	1.5	8.9	6.8	0.76	1.5	0.22	70	4.1	0.59	10.3	8.7	0.84	
14	Mag Cal 18	1.6	9	7	0.78	2	0.33	60	4.3	0.49	10.2	6.7	0.66	
15	Mag Cal 19	1.6	9.1	6.9	0.76	2	0.33	75	2.8	0.68	10.2	6.5	0.64	
* Vertical roof aspect ratio for elliptical honey chambers taken as roof thickness/long axis of honey chamber (cf. Roche et al. 2000)														
** Time after which motor was switched off in these experiments														
E = East; W = West; N = North; S = South														

of the model and the screw-jack lies to the ‘east’ (Fig. 2a). We first describe structures generated by regional-tectonic deformation (phase 1), then describe structures related to volcano-tectonic collapse (phase 2).

Strike-slip tectonic controls

With low opening angles ($< \sim 5^\circ$), Riedel shears (R-shears) with limited dip-slip displacement formed at $\sim 17^\circ$ to the velocity discontinuity. These locally delineated small transpressive pop-ups and/or narrow transtensive pull-aparts (Fig. 3a; Table 2a). Synthetic faults at lower angle R-shear and at P-shear orientations subsequently cut the earlier R-shears to form an anastomosing fault pattern encompassing rhombic gräben, half-gräben, and/or pop-ups. With moderate opening angles ($> \sim 5^\circ$), initial R-shears had greater dip-slip displacement (oblique-normal), and delineated rhombic gräben and/or half-gräben in an evenly-spaced, en-echelon array. With high opening angles ($> \sim 7^\circ$), an ‘axial’ graben system formed all along the velocity discontinuity, with R-shears mostly restricted to the graben margins (Fig. 3b; Table 2a). Where formed in the graben centre, R-shears defined relay ramps between sections of the axial graben system.

Regardless of opening angle, an almost vertical, gently sinuous or straight fault (Y-shear or ‘principal displacement zone’) later localised along the velocity discontinuity and cut all the above structures. Most strike-slip displacement in the model then transferred to this fault. In several experiments, particularly those with lower opening angles, the Y-shear developed by linkage of some lower-angle Riedel-like shears. Fractures in anti-Riedel (R’) orientation ($\sim 75^\circ$ to the shear zone) formed early in all the deformation sequences, but were generally ill developed and mostly confined to the floors of gräben or tops of pop-ups.

Strike-slip tectonics with a passive magma chamber

Overall kinematic development in this series resembled that in the strike-slip controls. With low opening angles, the honey chamber had little effect on regional-tectonic structures—apart from slightly widening the shear zone above it in one or two cases (Fig. 4a, b; Table 2b). With higher opening angles ($> 3\text{--}4^\circ$ —Fig. 5), however, normal faults localised around, and linked at depth to, the NE and/or SW chamber margins (Fig. 4d, e). These faults trended $30\text{--}45^\circ$ to the velocity discontinuity – almost perpendicular to the long axis of the theoretical incremental strain ellipse (Woodcock and Schubert 1994) – and delimited pull-apart-like gräben or half-gräben marginal to the shear zone axis. Gräben floors typically sloped toward the axis of the shear zone (Fig. 4e). Chambers centred on the velocity discontinuity tended to localise two normal faults (NE and SW);

offset chambers usually localised one normal fault (NE or SW). With very shallow chambers (0.5–1 cm depth) zero subsidence or even rare upward bulging occurred directly above the velocity discontinuity. Bulges trended NE–SW at around 45° to the shear zone – perpendicular to the short axis of the theoretical incremental strain ellipse – and overlaid similarly orientated, slightly sigmoidal ridges or folds in the chamber top surface. Development of chamber-localised pull-apart gräben diminished or ceased once the Y-shear cut through all structures. Upon excavation, most honey chambers were slightly sigmoidal and stretched roughly parallel to the regional NE–SW extension direction. Some also displayed a deformed basal ridge or a marginal ‘apophysis’, where honey was sucked down into or dragged along the shear zone (Fig. 4c, f).

Caldera collapse control experiments

Evacuation of circular honey chambers typically resulted in asymmetric, trapdoor-like collapses (Fig. 6a–c; Table 3a). Following a brief downsag phase, a reverse fault trace with a characteristic scarp morphology nucleated at an apparently random site on the chamber circumference (Fig. 6a). This reverse fault then propagated in both directions around the chamber edge from the most subsided roof section toward the least subsided section (‘trapdoor hinge’) sited opposite. The final reverse fault trace was not a smooth curve, but comprised several straight segments. Typically, a concentric peripheral zone of extensional cracking and faulting then formed (Fig. 6b). Material in the peripheral zone moved bodily inward toward and over the subsiding central caldera zone; this movement can only be accommodated along outward-dipping reverse faults around the central zone.

Evacuation of elliptical chambers (Fig. 6d–f; Table 3a) also caused sequential downsag, reverse fault formation, and asymmetric trapdoor-like subsidence. However, reverse faults consistently nucleated at or near the ends of the elliptical chamber’s short axis, and then propagated toward the ends of the chamber’s long axis (Fig. 6d). In Cal Stat 5 and 7, two reverse faults nucleated above or near both of the chamber’s short axis ends, but at different times during the course of subsidence. Consequently, the site of maximum subsidence shifted from one caldera side to the other. Both faults linked at the long axis ends to produce a single elliptical, but subtly polygonal, ring-fracture (Fig. 6d, e). Inward movement of the peripheral fault zone over the subsiding central caldera zone culminated in slumping of peripheral zone material from the over-steepened reverse fault scarp into the caldera centre (Fig. 6e).

The arcuate reverse faults were always closely associated with marginal ridges on the remnant honey chamber’s top surface (Fig. 6c, f). The more pronounced ridges frequently had vertical to steeply outward-dipping ($70\text{--}85^\circ$) inner

walls, just inside and parallel to which were outward-inclined furrows. The inner ridge walls and furrows thus represent traces of the reverse ring-faults that cut down into the chamber's top-surface. The ridges themselves perhaps represent chamber-remnant 'ring-dykes', as envisaged by Smith and Bailey (1968).

Strike-slip tectonics with passive magma chamber, followed by caldera collapse

Because of regional-tectonic elongation of the initially circular honey chambers, close similarities existed between collapse development in this set and that in elliptical chamber controls (Figs. 6 and 7; Table 3b). After early downsag, reverse faults again nucleated at the short axis ends of the underlying elliptical chamber's circumference and propagated toward the long axis ends (Fig. 7a–c). Reverse faults typically formed on one side of the chamber first, which again led to an asymmetric trapdoor-like subsidence style. Again, subsidence asymmetry often decreased after a second reverse fault formed above the opposite side of the chamber (Fig. 7d).

Important differences related to pre-collapse regional faulting existed between experiment sets, however (Table 4), mainly because of volcano-tectonic reactivations of regional-

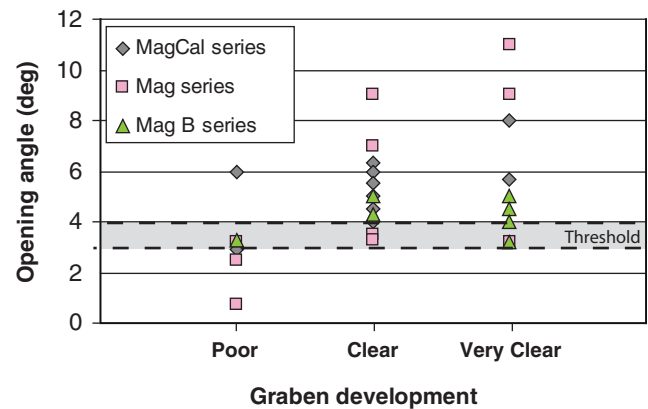


Fig. 5 Plot of opening angles in passive magma chamber experiments vs the development of chamber localised graben (categorised into poor, clear and very clear). A threshold, above which graben tended to localise, was reached at opening angles of 3–4°. At 95% confidence, mean opening angles for the 'clear and very clear' categories are indistinct from each other, but both are distinct from the 'poor' category

tectonic faults. Even with very high rates of scaled syn-collapse regional fault movement, such reactivations were clearly discernable, as scarp growth on regional faults within the limit of collapse influence far exceeded that elsewhere in the model. As noted above, collapse development in experi-

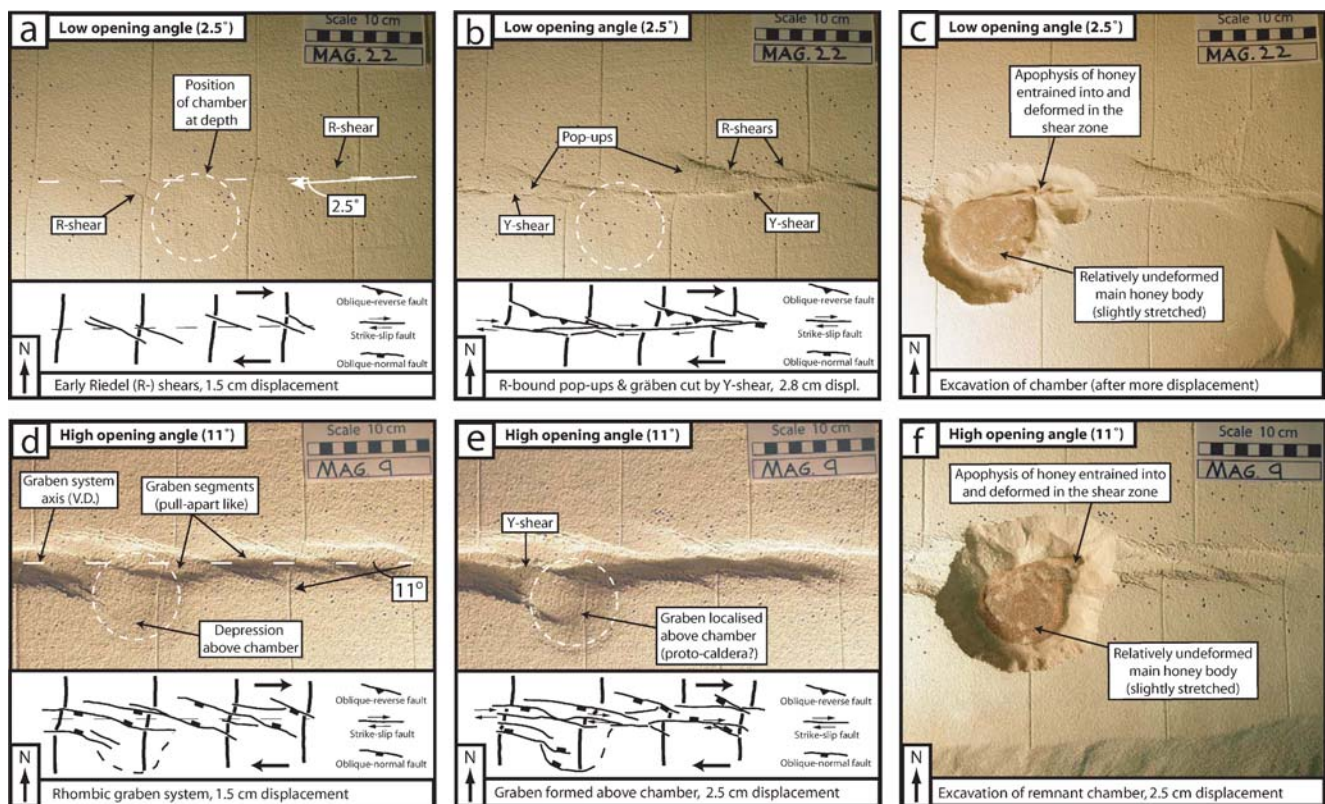
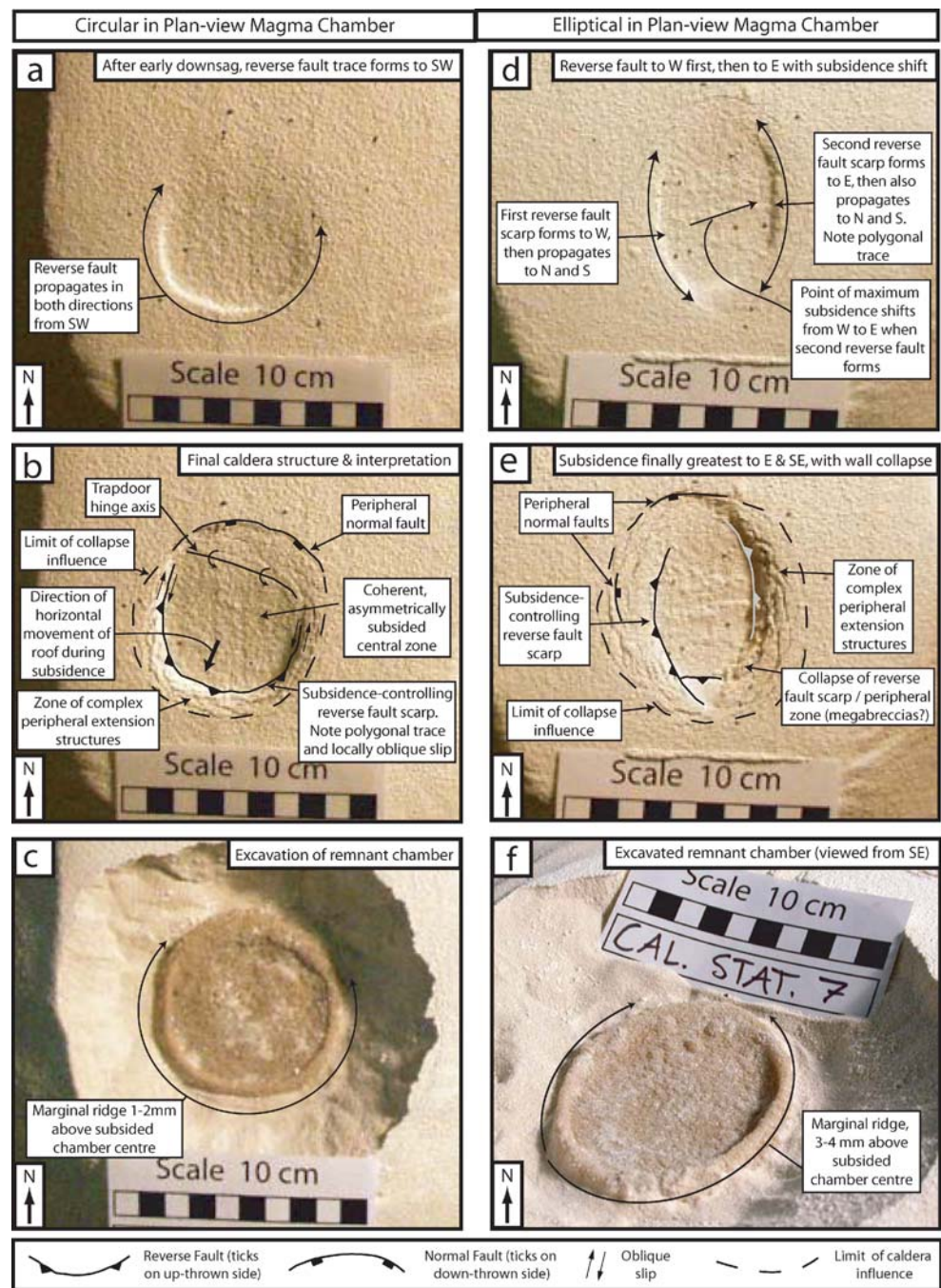


Fig. 4 Simulation of strike-slip deformation of brittle crust containing a passive magma chamber (light from SW). **a, b** At low opening angles, little effect was seen. **d, e** At higher opening angles (>~3–4°), pull-apart like graben formed marginal to and above the magma

chamber. **c, f** Honey chambers are slightly elongated parallel to regional stretching direction (cf. Fig. 3) and locally more intensely deformed along the Y-shear. Extension across the chamber localises as graben/normal faults at the rheological change along the chamber edge

Fig. 6 Evolution of caldera collapse into circular and elliptical magma chambers (light from E). Circular: **a** Following early sagging and peripheral cracking, a reverse fault trace appears at a random point above the circular chamber's circumference, and propagates bi-directionally toward the opposite side. **b** The final structure is an asymmetric (trapdoor-like) caldera with a hinge zone opposite the point of reverse fault initiation. **c** A ridge related to the reverse fault borders the underlying magma chamber remnant. Elliptical: **d** After sagging, reverse fault traces appear consecutively above either short axis ends of the elliptical chamber circumference. **e** Both faults propagate toward the chamber's long axis ends, where they link. Again, the final caldera is asymmetric (trapdoor-like) with a hinge located around the chamber long axis end. **f** Vertical to slightly outward-dipping ridges related to the reverse faults again mark the underlying magma chamber remnant



ments with or without syn-collapse regional displacement (the latter is geologically more realistic) was essentially the same (Figs. 7, 8 and 9).

Pre-collapse regional faulting had two main effects on caldera development. Firstly, parts of the pre-collapse structural grain, usually Riedel shears and/or chamber-localised faults close to the chamber margins, were reactivated to accommodate caldera floor subsidence (Figs. 6, 7, 8 and 9; Table 4). Generally, such reactivated regional faults also had tangential orientations to the collapse centre, whereas un-activated faults had non-tangential orienta-

tions. Faults located outside the chamber margin, but within the influence of collapse, reactivated as peripheral normal faults (Figs. 7a, b and 8a). Regional faults located inside, but close to, the chamber margin, linked with adjacent volcano-tectonic reverse faults and reactivated as bounding faults to the central zone (Figs. 7d, e and 8a, b). A rare exception to this pattern is seen in Fig. 8e, where a Riedel shear lying inside the chamber margin reactivates as a peripheral normal fault. In this case, however, the reactivated Riedel shear also lies in the typically extensional hinge zone of an asymmetrically subsiding roof.

Secondly, volcano-tectonic reverse faults were arrested at sharp corners defined in the magma chamber margins by regional-tectonic faults, typically Y-shears (Table 4; Figs. 7d, e and 8e, f). In contrast, reverse-fault propagation was unaffected where chamber margins lacked such sharp regional-fault defined corners (Fig. 8b, c). Reverse fault arrest was commonly associated with a sharp bend of the marginal ridge into the regional fault (typically Y-shear) trend, with little or no change in ridge height. This may be evidence for local deep-level transfer of volcano-tectonic displacement from arrested reverse fault onto the regional fault (Fig. 7f). Similar deep-level displacement transfer is inferred along a blind reverse fault in Fig. 8f. The typical upwards-decreasing displacement on such reverse faults (cf. Roche et al. 2000; Kennedy et al. 2004) means that such reactivation could occur at depth and not noticeably show at the surface.

In contrast to the smooth floor surfaces of central caldera zones in non-tectonised control experiments, central zone floor morphology in caldera experiments following regional deformation was irregular (Figs. 7d, e; 8a, b, d, e and 9a, b). Dissection of the central zone by regional structures formed a pre-collapse topography comprising regional fault-controlled segments of varying structural level. During subsequent

caldera subsidence, this fault-controlled topography subsided coherently, however (Figs. 7a, d and 9a, b). No significant syn-collapse motion (scarp growth) was noted on the segment-bounding regional faults.

Cross-sections (Fig. 9c, d), demonstrate the connection of the reactivated chamber-localised normal faults to the honey chamber margin. Similarly, the outward dips and reverse sense of the faults bounding the central caldera zone are also visible; these also connect at depth to the chamber margin. Note also the upward decreasing displacement on the volcano-tectonic reverse faults and downward decreasing displacement on the volcano-tectonically reactivated normal faults. Gently sagged pre-collapse strata in the central caldera zone also display offsets along regional-tectonic faults; these offsets predate caldera collapse, however.

Discussion

We firstly discuss the generation of structures during experimental regional-tectonic transtensive shear (deformation phase 1). We then focus on the impact of such structures upon the development of experimental volcano-

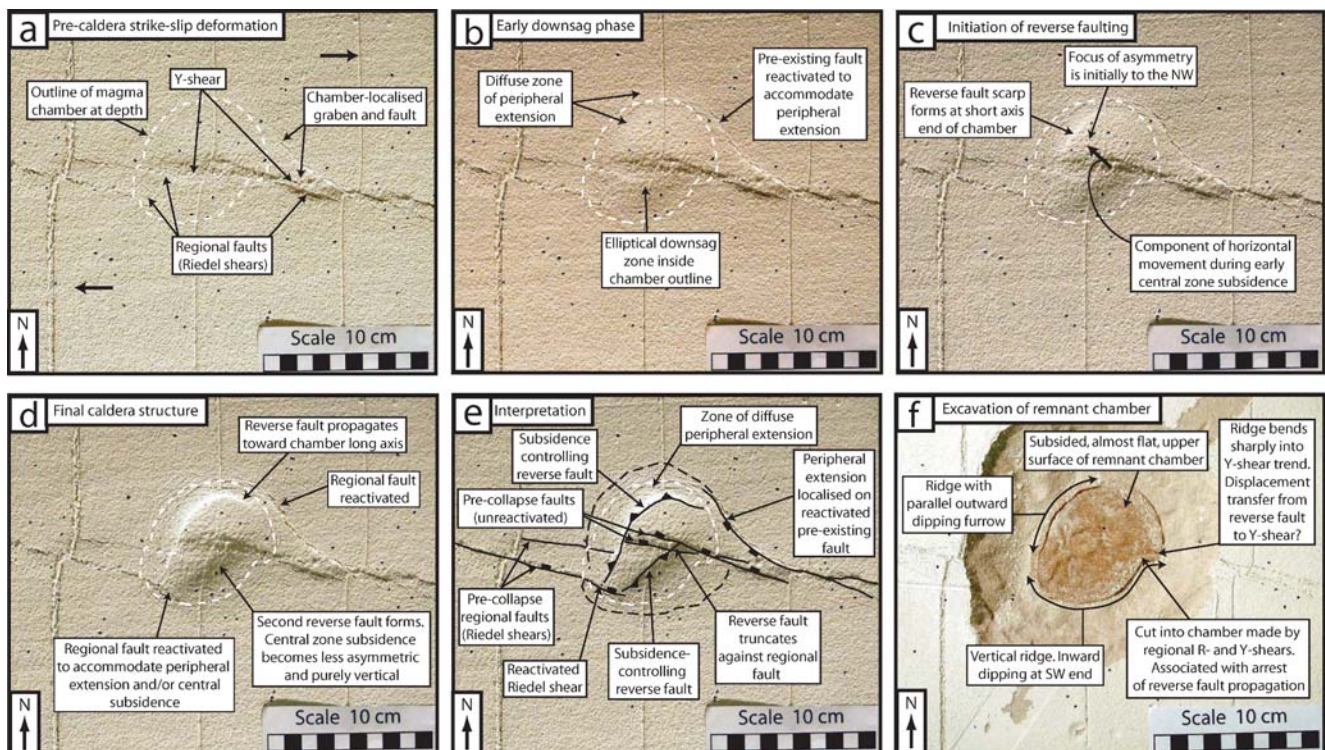


Fig. 7 Caldera collapse evolution following regional strike-slip deformation (MagCal 2—light from SE). **a** Pre-collapse regional structures include Riedel shears, a chamber-localised graben fault, and a partial Y-shear. **b** Collapse begins with down-sag and peripheral extension, the latter taken up along new fractures and/or the pre-collapse chamber-localised fault just beyond the chamber margin. **c** A reverse fault appears above the short axis end of the chamber, and **d**

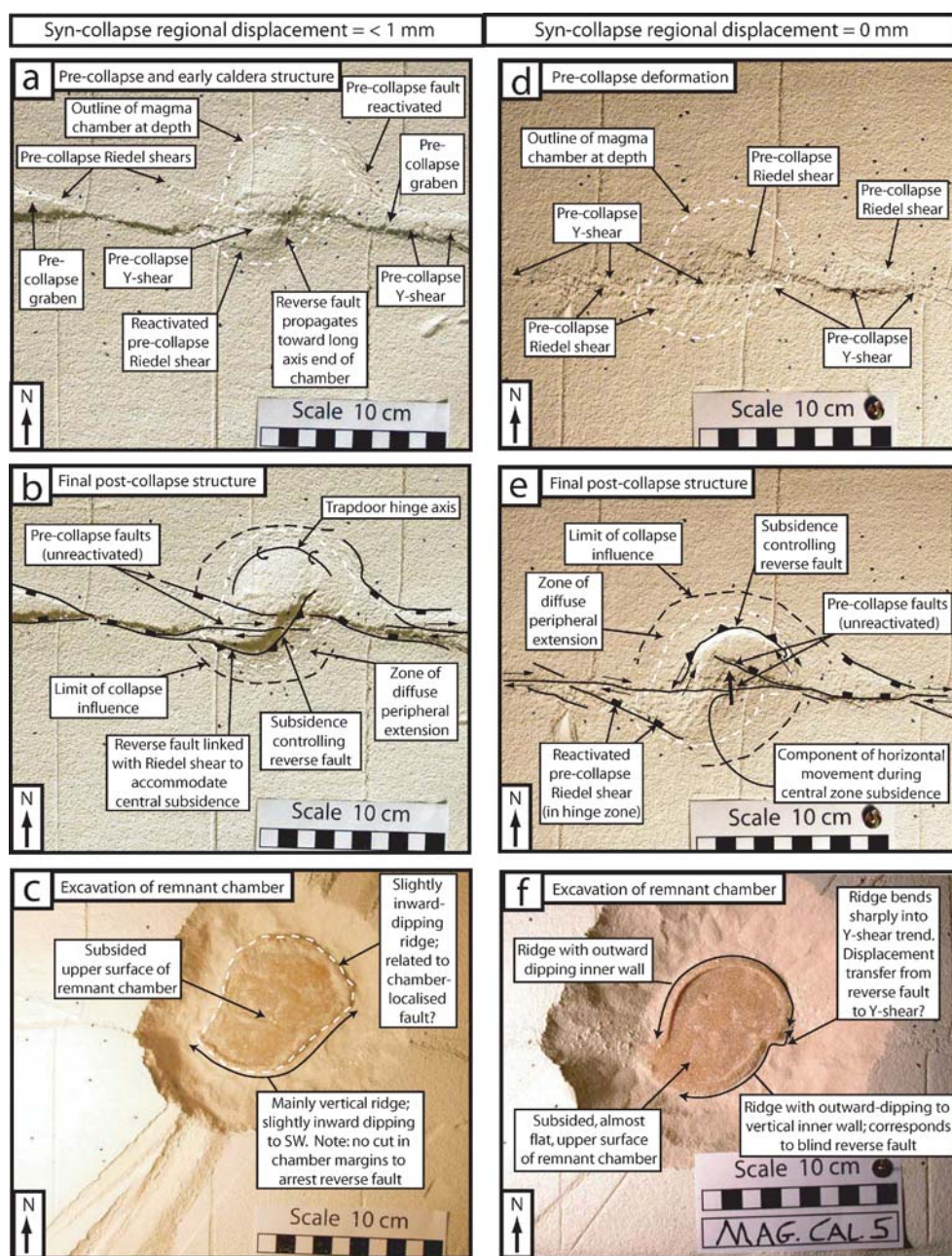
propagates to the long axis end, where a pre-collapse Riedel-shear reactivates. **e** A second reverse fault appears on the opposite side of the chamber, but its NE-ward propagation halts upon intersection with Riedel- and Y-shears. **f** Excavation of the chamber remnants reveals that the arresting regional faults define a sharp bend in the chamber margin at this point. Syn-collapse regional displacement was <1 mm

Table 4 Observations on regional-tectonic and volcano-tectonic fault interactions during caldera collapse

	Syn-collapse regional motion (cm)	Reactivation of pre-collapse regional faults at surface?	Position of reactivated faults (central zone vs. peripheral zone)	Reverse faults arrested at corners cut by regional faults?	Displacement transfer from reverse fault to regional fault?
MagCal 5	0.0	Yes, but subtle. R-shear to SW	Outside chamber margin (peripheral fault)	Yes. Reverse fault to NW arrested against Y-shear	Yes. Marginal ridge to SE bends into Y-shear corner
MagCal 14	0.0	Yes. R-shears to (1) NE and (2) SW	(1) Outside chamber margin (peripheral fault) (2) Outside chamber margin (peripheral fault)	Yes. Reverse fault to NW and SE arrested against R-shear	Unclear
MagCal 16	0.0	Yes. Chamber-localised faults to (1) NW and (2) SE	(1) Outside chamber margin (peripheral fault) (2) Outside chamber margin (peripheral fault)	No reverse faults formed (just sag)	N/A
MagCal 17	0.0	Yes. Chamber-localised faults to (1) NW and (2) SE	(1) Outside chamber margin (peripheral fault) (2) Outside chamber margin (peripheral fault)	No. No corners	N/A
MagCal 18	0.0	Yes. Chamber-localised fault to SW	Inside chamber margin (central caldera fault?)	Unclear as cross-sectioned, not excavated	N/A
MagCal 19	0.0	Yes. Chamber-localised faults to (1) NE and (2) SW	(1) Outside chamber margin (peripheral fault) (2) Outside chamber margin (peripheral fault)	Unclear as cross-sectioned, not excavated	N/A
MagCal 2	<0.1	Yes. (1) Chamber-localised graben fault to NE and (2) R-shear to SW	(1) Outside chamber margin (peripheral fault) (2) Inside chamber margin (central caldera fault?)	Yes. Reverse fault to SE arrested against Y- & R-shears	Yes. Marginal ridge to SE on chamber bends sharply into Y-shear corner
MagCal 3	<0.1	Yes. (1) Chamber-localised graben fault to NE and (2) R-shear to SW. Note: most re-activation after motor stopped	(1) Outside chamber margin (peripheral fault) (2) Inside chamber margin (central caldera fault)	No. No corners cut	No

Summary of observations on regional-tectonic and volcano-tectonic fault interactions during caldera collapse. Syn-collapse regional motion values were measured not estimated

Fig. 8 Further examples of caldera collapse following regional strike-slip deformation (light from the SE in **a, b, d, e** and from SW in **c, d**). In MagCal 3, **a** peripheral extension again partly localised on a pre-collapse graben fault to the NE, **b** the reverse fault here propagates unimpeded toward both long axis ends and links with a pre-collapse Riedel-shear in the SW. **c** Excavation reveals no corners in the chamber margin. In MagCal 5, **d, e** the reverse fault is arrested at a Y-shear defined corner in the W, **f**, and a Riedel shear located just inside the chamber margin reactivates in the SW. Note the ridge to the E bends sharply into Y-shear orientation. Syn-collapse regional displacement: MagCal 3 <1 mm; MagCal 5=0 mm



tectonic caldera collapse (deformation phase 2) and deduce implications for the influence of regional strike-slip structures in natural calderas.

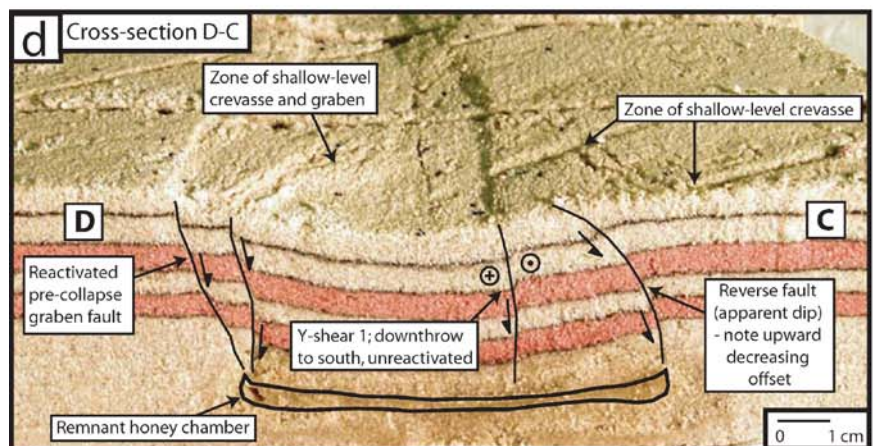
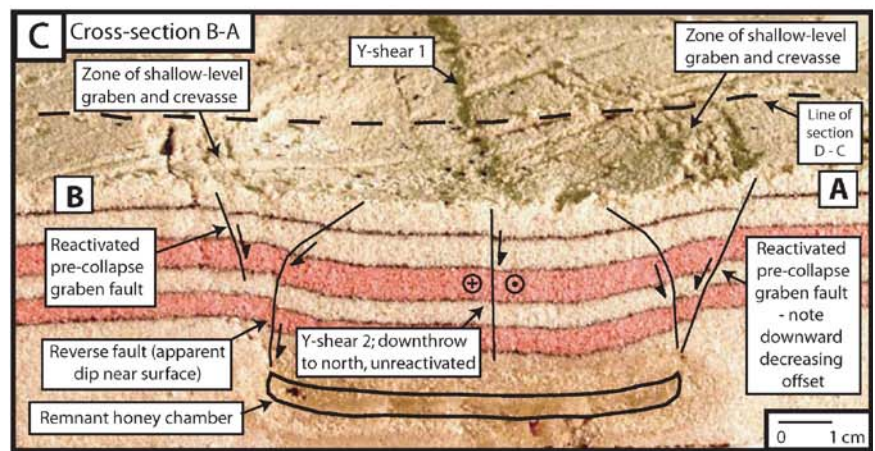
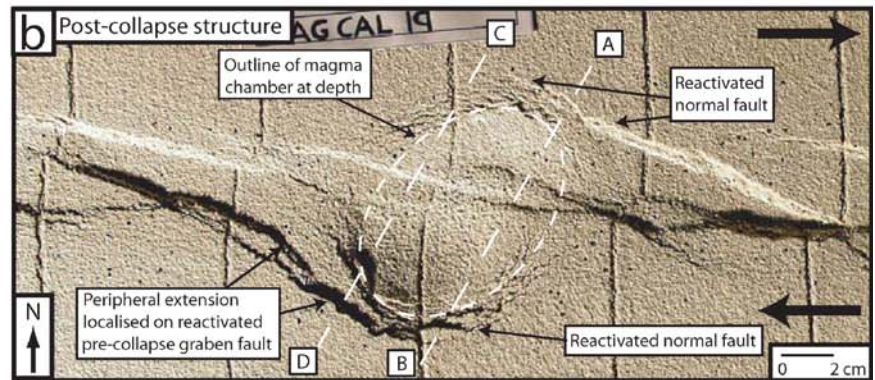
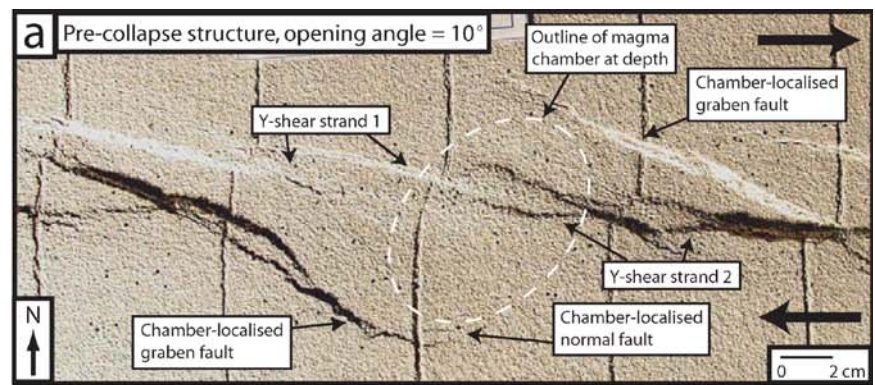
Regional-tectonic structures related to strike-slip and transtensive shear

Development of strike-slip structures in a homogeneous medium

Fault geometries and their sequential development during strike-slip deformation of homogeneous sand/gypsum piles matched those produced in previous experimental inves-

tigations of strike-slip and transtensive faulting (e.g. Schöpfer and Steyrer 2001 and references therein). These studies, report similar formation of en-echelon Riedel shears at an angle of $\phi/2$ (where $\phi \sim 37^\circ$ = angle of internal friction of sand) to the maximum regional stress direction, σ_1 , ($\sim Z$ -direction of incremental strain ellipse—Fig. 3) followed by generation of Y- and P-shears, which link as a through-going ‘principle displacement zone’. With low components of dilation, both compressive and extensional structures form locally at restraining and releasing bends along the principle displacement zone. With higher components of dilation, compressive structures are absent, and a broader zone of deformation forms as an axial graben

Fig. 9 Cross-sections of a model caldera formed after regional strike-slip tectonism (Mag Cal 19). **a** Pre-collapse structure (light from SW). **b** Post-collapse structure—note reactivation of regional normal fault to SW and NE. Regional faults in caldera central zone were again unreactivated. **c, d** Cross sections along lines *B–A* and *D–C*, viewed from oblique angle to show relationship with surface deformation. Reverse faults are not well expressed at surface due to upward-decreasing displacement. Note that all structures with volcano-tectonic displacement converge on the honey chamber margin



system with segment-linking relay ramps in Riedel orientation, as seen in our experiments.

Development of pull-apart-like structures and elongation of pre-collapse magma chambers

The geometries and sequential development of structures localised around the passive honey chambers during strike-slip deformation are akin to structures formed in analogue studies of pull-apart basin formation (e.g. Dooley and McClay 1997; Basile and Brun 1999). Previous model pull-aparts differed from our pull-apart-like structures, in that the former developed above a pre-defined releasing bend or step-over between two master fault strands (Y-shears), whereas the latter formed above a fluid body. Nonetheless, these studies also report early formation of oblique-normal faults at 30–65° to a basal velocity discontinuity (sub-perpendicular to the incremental strain ellipse long axis). These oblique-normal faults are termed ‘sidewall faults’ to the pull-apart basins (Dooley and McClay 1997), which also display late-stage development of a through-going ‘principal displacement zone’ (Y-shear in our models)—Dooley and McClay 1997; Basile and Brun 1999).

Field studies demonstrate that molten to semi-solidified granite plutons can undergo substantial rotation and elongation due to regional strike-slip tectonism during and after their emplacement. The Caledonian Rannoch Moor granite, Scotland, was emplaced at mid-crustal levels into a diffuse sinistral strike-slip regional tectonic regime (Fig. 10a—Jacques and Reavy 1994). A sigmoidal swing in steeply-dipping pre-full crystallisation (PFC) magmatic foliations in Rannoch Moor is interpreted as evidence for synchronous inflation and regional-tectonic rotation and elongation of the pluton (Jacques and Reavy 1994). The PFC magmatic fabric is weakly overprinted by crystal plastic strain fabrics, which indicate further, late-stage, solid-state stretching of the pluton parallel the maximum extension direction of regional strain ellipse (Jacques and Reavy 1994). A similar emplacement history is inferred for the nearby, contemporaneous, similarly elongate, but shallower level (3–6 km) Etive pluton (Jacques and Reavy 1994). The Caledonian Ardara granitic pluton, Ireland, also shows steeply dipping PFC magmatic foliations concentric to its margins (Molyneux and Hutton 2000—Fig. 10c). Distribution of flattening strain within the Ardara pluton indicates that it inflated from a near-central ‘injection point’ sited laterally to a major (later?) sinistral shear zone (Molyneux and Hutton 2000). Like our honey chambers sited laterally to the velocity discontinuity (Fig. 10b), the pronounced ‘tail’ of the Ardara pluton is considered to have formed by deformation in the intersecting major shear zone (Molyneux and Hutton 2000—Fig. 10b, c). This deformation is seen as a late-stage high-temperature solid-state

strain fabric that is concentrated along the southern and north-eastern margin of the pluton. Like Rannoch Moor and Etive plutons, the Ardara pluton is elongate parallel to the direction of horizontal extension in the regional sinistral shear. The long axes of plutons forcefully emplaced into shear zones in past analogue experiments also tend to track the direction of maximum extension in the regional finite strain ellipse (Roman-Berdiel 1999; Corti et al. 2005). The overall geometry and elongation of magma chambers prior to caldera collapse in our experiments may thus closely reflect that of many magma chambers in natural strike-slip systems.

Can long-lived, shallow-level magmatic centres localise faults and pull-apart-like graben?

The pull-apart-like graben in our models formed through localisation of regional-tectonic strain (elongation and rotation) at the rheological discontinuity represented by the honey chamber’s edge. Whilst the regional tectonic framework (strike-slip faults, shear zones, releasing bends and/or step-overs) likely provides the initial pathways for siting and emplacing magmatic centres (Hutton and Reavy 1992), the experiments here indicate the possibility that the rheological discontinuity represented by a semi-solidified and long-lived magmatic system may exert a localised post-emplacement influence on the subsequent development of the regional fault system around it. From similar experimental results, Girard and van Wyk de Vries (2005) explained the structural relationship between the Managua graben and the adjacent Masaya volcanic system in this way. Both structures are currently active and located in the Nicaraguan depression, and are proposed to reflect the localisation of a pull-apart graben by a deep-level basic intrusive complex. Our results support Girard and van Wyk de Vries’s (2005) proposals that: (a) such pull-apart localisation may occur if the transtensive component in the strike-slip regime is sufficiently high (opening angle of >3–4°—Fig. 5), and (b) a similar effect might be possible above shallower-level magmatic centres.

An example of the latter may be the Pleistocene Mt. Guardia-Fossa ‘volcano-tectonic depression’, Italy (Fig. 11a). This structure lies within the active dextral Tindari-Letojanni shear zone, and apparently formed during a long period of volcanic quiescence. Ventura et al. (1999) therefore proposed that the depression’s arcuate bounding faults resulted from “re-orientation of tectonic stress around a shallow reservoir and/or inside the pull-apart”—i.e. perhaps by regional-tectonic strain localisation around a magma chamber. The 1.4 Ma Hopong Caldera (Fig. 11b), Indonesia, lies beside the active Tor Sibohi strand of the dextral Great Sumatran Fault Zone, and the geothermally-productive Sarulla Graben (Hickman et al. 2004). Unlike other volcanoes along this strand, e.g. Sibualbuali volcano

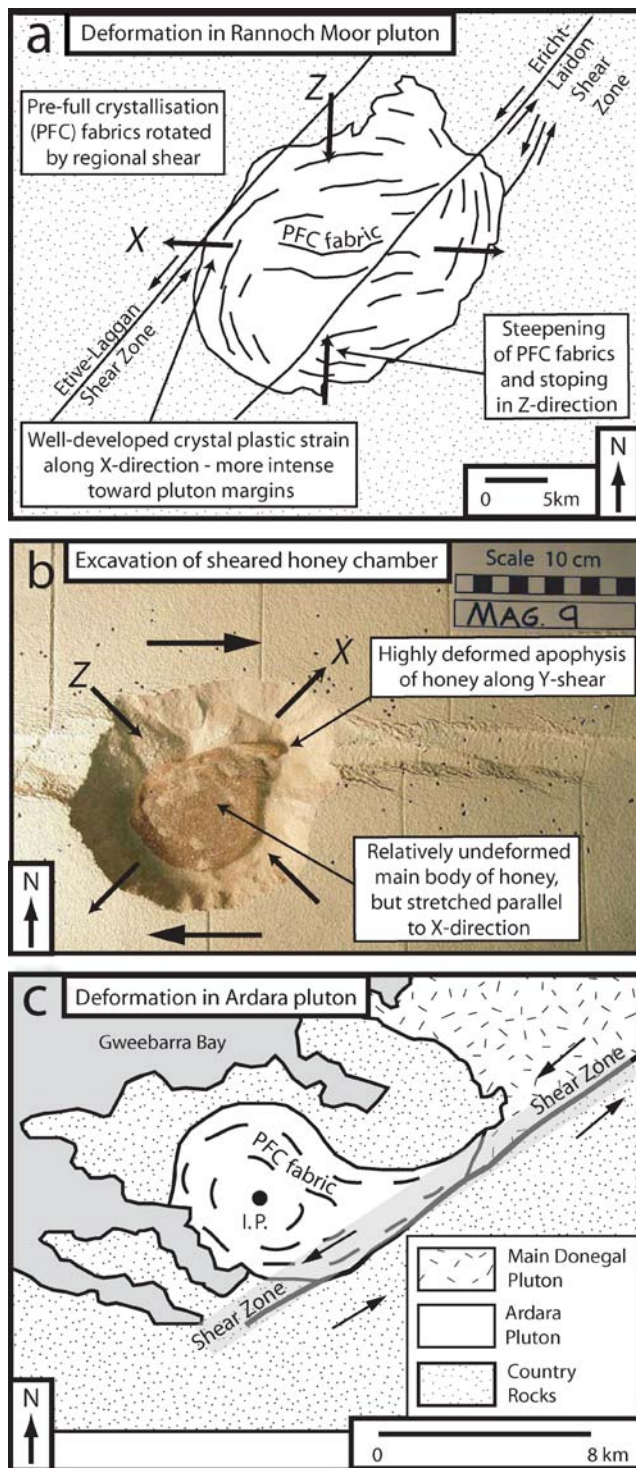


Fig. 10 **a** Sited and partly shaped by regional faults, the Rannoch Moor granite, Scotland, was deformed and elongated prior to full crystallisation by transpressive regional-tectonics (adapted from Jacques and Reavy 1994). **b** In the models, honey chambers are similarly elongated and with respect to the regional shear, and extensional structures consequently localise along their margins. **c** The Ardara pluton, Ireland, is similarly elongated with respect to the regional shear sense. During and/or shortly after its emplacement at a low strain injection point (I.P.), Ardara pluton developed a strongly deformed 'tail' where intersecting the Donegal Shear Zone (adapted from Molyneux and Hutton 2000)

(Fig. 11b), it is not clear if a step-over or bend in the strike-slip system played any role in siting the Hopong caldera. The structural setting, relationships, and morphology of the Hopong-Sarulla system are remarkably similar to those produced in our passive chamber with strike-slip models (Fig. 11c), however. We therefore hypothesise that, in addition to later volcano-tectonic caldera collapse, localisation of regional-tectonic faults around this magmatic centre may have played a role in its evolution, but more detailed appraisal of this issue is beyond the scope of the present work.

Volcano-tectonic structures and displacements related to catastrophic caldera collapse

Caldera collapse without regional-tectonic influence

The structural evolution of 'simple' (single reservoir, single subsidence event) collapse due to honey chamber deflation mirrored that in previous experimental caldera studies, but displayed some noteworthy extra details. Firstly, reverse faulting above circular chambers initiated at an apparently random point around the chamber circumference, though subtle lateral variations in roof loading possibly influenced the exact location in each case (cf. Roche et al. 2000). In contrast, reverse faulting above elliptical chambers consistently initiated above the short axis ends of the chamber circumference, and propagated around to the long axis ends. This fault evolution reflects that at Long Valley caldera, California (Hildreth and Mahood 1986) and may thus be characteristic of subsidence into elliptical chambers (Roche et al. 2000). Secondly, our study is the first to report reversals of subsidence symmetry in experiment, though only above an elliptical honey chamber. We tentatively attribute them to the faulting pattern particular to elliptical subsidence and perhaps to the sensitivity of the low-viscosity honey to subtle variations in roof loading. Carr and Quinlivan (1968) inferred a similar symmetry reversal at Timber Mountain caldera, Nevada. Thirdly, arcuate reverse faults were subtly polygonal, rather than perfectly smooth curves (see also Kennedy et al. 2004). Past explanations for polygonal caldera ring faults have included: (1) the intersection of fractures related to doming and collapse (Komuro 1987) and (2) the reactivation of regional-tectonic faults (Nappi et al. 1991; Orsi et al. 1996). However, we agree with Kennedy et al. (2004) that the generation of polygonal ring faults may simply be more inherent on all scales to the caldera collapse process than hitherto recognised. If other mechanisms are invoked to account for a linear ring-fault segment, they require clear demonstration—e.g. regional-tectonic fault reactivation deduced from alignment and/or continuation of a segment with a regional fault.

Reactivation of pre-collapse regional-tectonic faults during collapse

Model collapse with regional-tectonic influence generally resembled that without regional-tectonic influence. This result supports inferences, from the generally sub-circular to elliptical caldera shapes in nature, of a magma chamber dominated syn-collapse stress/strain field (Lipman 1997; Roche et al. 2000). Pre-collapse regional-tectonic faults nonetheless substantially affected the experimental volcano-tectonic caldera structures in two ways. Firstly, regional-tectonic faults orientated tangentially to the chamber centre and located just inside the chamber margin linked with arcuate volcano-tectonic reverse faults and re-activated to become bounding faults to the central caldera zone (Figs. 7d, e and 8b—see also Acocella et al. 2004; Holohan et al. 2005). Tangentially orientated regional-tectonic faults located beyond the chamber margin usually reactivated as bounding faults to the peripheral caldera zone (Figs. 7b; 8a, b and 9a, b). Secondly, where orientated non-tangentially, but defining corners in the chamber margins, regional faults often abruptly halted reverse fault propagation (Figs. 7d, e

and 8e—cf. Roche et al. 2000) and locally reactivated to accommodate some of the volcano-tectonic displacement. Regional-tectonic faults in non-tangential orientations and those located above the centre of the chamber did not otherwise noticeably reactivate during collapse.

In nature, the often highly elongated calderas in strike-slip zones (e.g. Toba, Ranau) very likely formed from non-circular reservoirs with variable regional fault control (e.g. Ardara pluton). Consequently, and as seen in experiment, elongate magma chamber geometry may primarily control the spatial and temporal development of subsidence-controlling faults (and associated vents) at these calderas. The influence of regional-tectonic faults on this volcano-tectonic development should depend largely on the extent to which they: (a) are tangential to the collapse centre, and/or (b) define or coincide with the magma chamber margins. Such regional faults can be viewed as optimally orientated and positioned for reactivation, as collapse-related strain (radially-directed extension and contraction, and vertical shear) mainly localises around the chamber margins (see also Roche et al. 2000; Kennedy et al. 2004; Acocella et al. 2004; Holohan et al. 2005).

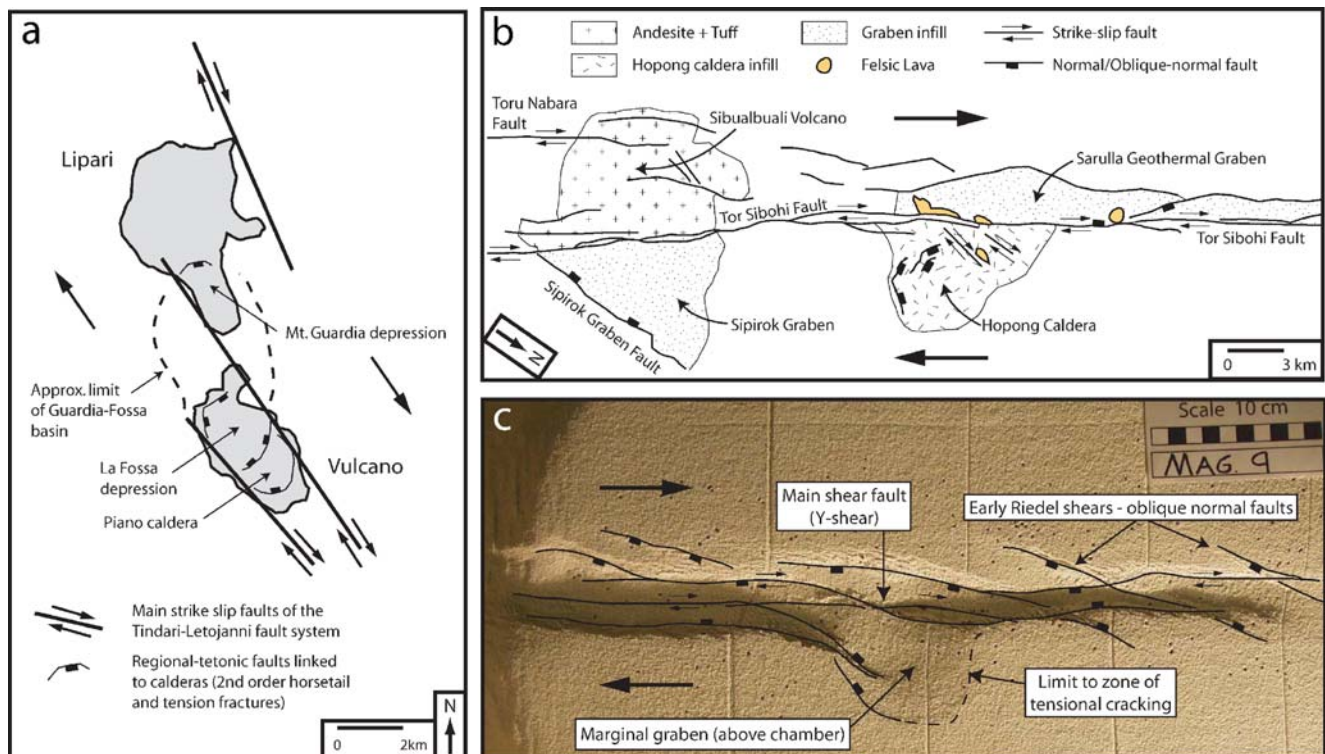


Fig. 11 **a** The islands of Lipari and Vulcano are sited at a step-over in the Tindari-Letojanni strike-slip system (adapted from Ventura et al. 1999). The Guardia-Fossa depression is a caldera-like structure interpreted to have formed mainly from regional-tectonic subsidence, rather than catastrophic collapse. The depression's arcuate bounding faults are believed to be from regional stress/strain localisation on the

Guardia-Fossa magmatic system's margins. **b** Arcuate normal fault structures preserved at the Hopong caldera, which lies beside the Tor Sibohi strike-slip fault, Indonesia (adapted from Hickman et al. 2004), are similar to those localised above passive honey chambers positioned laterally to a shear zone (**c**)

Effects of pre-collapse regional-tectonic faults on collapse style (mode)

Branney and Kokelaar (1994) define piecemeal as “composed of many pieces; bit by bit” and suggest this definition “is useful to describe both the *morphology* of calderas with highly fragmented floors and the *mode of collapse* in which different parts subside at different times or rates” (our italics). Using the term ‘piecemeal’ to describe the floor morphology is potentially confusing, however, because it blurs the relationships between floor complexity and the different structural processes that can generate such complexity—e.g. regional-tectonic subsidence, volcano-tectonic collapse, landsliding, etc. Moreover, piecemeal subsidence as demonstrated at Scafell caldera (Branney and Kokelaar 1994) implicitly carries with it a genetic link between the complexly block-faulted floor morphology and differential, *syn-eruptive*, *volcano-tectonic* subsidence along the block-defining faults. We therefore apply the term ‘piecemeal’ to *mode of collapse* only, whereby the caldera floor (=pre-collapse palaeo-surface) subsides as multiple, differentially-sinking fault blocks during volcano-tectonic deformation.

This distinction is important because, in experiments, the peripheral caldera zone floor usually broke up along a complex array of volcano-tectonic extensional faults—i.e. could be interpreted as subsiding in piecemeal style. Conversely, whilst the central zone caldera floor commonly comprised several regional-fault-bound, differentially-subsided segments, this differential subsidence seems to have occurred solely during pre-collapse regional-tectonic deformation. During volcano-tectonic collapse, the central zone floor apparently subsided coherently; no movement (scarp growth) was observed on the segment-bounding R- and Y-shears (Figs. 7a–d; 8a, b, d, e; and 9a, b). Our experiments thus show that a fragmented *central* caldera zone floor can arise predominantly through *pre-collapse* regional-tectonic faulting, the effects of which may be subsequently preserved by essentially coherent caldera subsidence.

In nature, a coherently-subsided, fault-controlled palaeotopography will produce abrupt, fault-scarp-defined lateral changes in accommodation space and hence in caldera infill thickness—especially with topography-blanketing ignimbrites. Such thickness changes might be misinterpreted as evidence of syn-eruptive growth faulting. This problem may be most acute where thickness changes are relatively small (a few 10s–100 m) and where floor and infill structure is very poorly-exposed and mainly inferred—e.g. from borehole data and/or gravity anomalies. Alternatively, because pre-collapse (and post-collapse) regional-tectonics can generate significant differential movement between caldera floor blocks (as inferred at Glencoe caldera—Moore and Kokelaar 1998), the magnitude of any purely volcano-tectonic subsidence on a regional structure may be overestimated. In the absence of

unequivocal evidence for reactivation of pre-collapse faults as syn-collapse growth-faults (cf. Branney and Kokelaar 1994), as seen in places at Glencoe caldera (Moore and Kokelaar 1998—see below), caution is advised when estimating the extent to which regional-fault-defined changes in caldera fill thickness, and/or offsets of the caldera floor, reflect *volcano-tectonic* motion.

Moore and Kokelaar’s (1998) landmark study of the Caledonian Glencoe volcano, Scotland is to date the most detailed analysis of the influence of regional-tectonic faulting in caldera development (Fig. 12a). Within a probably sinistral strike-slip regime, extension and/or trans-tension at Glencoe occurred along several orthogonally-intersecting regional-tectonic faults (Moore and Kokelaar 1998—Fig. 12a). The regional-fault-dissected caldera floor and a tightly-constrained caldera infill succession (Fig. 12b) are preserved inside a large-displacement (>700 m) ring fault system that is locally steeply outward-dipping (Kokelaar and Moore 2006—Fig. 12a). From thickness changes in ignimbrites across the regional faults, ponding of ignimbrites against regional fault scarps, and local intercalation of fault-scarp-derived breccias in ignimbrites, Moore and Kokelaar (1998) inferred a complex history of differential and incremental volcano-tectonic subsidence (i.e. piecemeal collapse) of caldera floor blocks along the regional-tectonic faults.

The area inside the ring fault system at Glencoe may be comparable to the central caldera zone in our experiments, and hence volcano-tectonic reactivations along regional faults would seem to be possible there in nature—in contrast to the experimental results. Direct comparison between our experiments and Glencoe caldera, though pertinent, is difficult, however. Unlike in our single-collapse experiments, volcano-tectonic subsidence at Glencoe is thought to have occurred during several major eruptive/collapse events, which punctuated a protracted period (maybe 0.5 Ma—Moore and Kokelaar 1998) of pre- and post-collapse regional-tectonic faulting and differential graben subsidence. Moreover, the role played by ring faulting in accommodation of volcano-tectonic subsidence, important in experiment, is rather uncertain at Glencoe (Moore and Kokelaar 1998). We nonetheless consider three possible explanations of disparities between the observations in experiment and at Glencoe.

Firstly, the apparent absence of regional fault reactivation above the experimental chamber’s centre may largely relate to the boundary conditions imposed. Previous experimental studies (cf. Roche et al. 2000; Kennedy et al. 2004) consistently related low thickness/diameter ratios of the roof to more coherent collapse style in the central zone. In contrast, higher thickness/diameter ratios result in less coherent central collapse. Furthermore, a flat upper surface of the magma chamber tends to restrict reverse faulting to the chamber margins, whereas a curved

convex-upward upper magma chamber surface promotes additional reverse faults in the central caldera zone (cf. Roche et al. 2000; Walter and Troll 2001; Kennedy et al. 2004). The coherent central caldera zones in our experiments may thus relate to an overriding control from the low roof thickness/diameter ratios and the flat tops of our honey chambers. More incoherent (piecemeal) central zone collapse, with reactivation of the regional faults, might have developed with higher roof thickness/diameter ratios and/or a curved chamber top-surface.

Secondly, disparity may be a function of model resolution, and single collapse events at Glencoe may to some extent be consistent with the single magma chamber experimental model. The inferred collapse-related reactivations of regional faults in the central zone of Glencoe caldera range from a few 10s of meters to just over 100 m (Moore and Kokelaar 1998), which scales to less than 0.5 mm in experiments. Regional fault reactivations in the model central zone may thus have been comparable to those in nature, but too small for us to resolve. If this is the case, then we might expect that volcano-tectonic reactivation of pre-collapse regional structures in a down-sag dominated central caldera zone in nature should be of small displacement (<100 m) relative to displacements on main ring faults and/or chamber-bounding regional faults (100s of meters to >1 km). Such a scenario seems compatible with, for instance, the inferred collapse history during emplacement of the >200 m thick Upper Three Sisters Ignimbrite (Fig. 12b—cf. Moore and Kokelaar 1998). Differential subsidence along regional faults is inferred to have accommodated ~40–50 m of the total 200 m of subsidence, with the majority accommodated by coherent sagging and probable ring faulting (Moore and Kokelaar 1998).

Thirdly, the pattern of differential volcano-tectonic subsidence of regional-fault-bound blocks at Glencoe may relate to several spatially and temporally discrete sub-caldera magma chambers. Indeed, Moore and Kokelaar (1998) suggested this possibility to account for differential subsidence at Glencoe. If regional faults delimited each chamber, their reactivation during eruption would be compatible with the focusing of regional fault reactivation at the experimental magma chamber margins.

Reactivation of regional tectonic structures has also been suggested to promote an asymmetric ‘trapdoor’ subsidence style (Lipman 1997; Riller et al. 2001; Ramelow et al. 2006). As this style characterised experiments with and without regional faults, we primarily ascribe the trapdoor-like subsidence in our experiments to the influence of low roof thickness/diameter ratio (cf. Kennedy et al. 2004). Although regional-tectonic faults did not promote asymmetric collapse in experiment, we note that they occasionally facilitated it (e.g. Figs. 8b and 9b).

Influence of regional strike-slip structures on caldera development in pull-apart-like settings

The general evolutions and geometries of calderas proposed to have formed in pull-apart structures show close similarities to our experiments. From patterns of active and inactive (recent) faulting, Bellier and Sebrier (1994) inferred that the 0.074 Ma Toba and 0.55 Ma Ranau calderas, Indonesia, formed in contemporaneous, but presently inactive, pull-apart graben. Firstly, a step-over or relay in the dextral Great Sumatran Fault Zone gave rise to a regional-tectonic pull-apart graben. Early volcanic activity at Toba and Ranau occurred around the pull-apart’s ‘sidewall’ normal faults (Fig. 13a). Secondly, the sidewall faults of the pull-apart graben reactivated to partly delimit volcano-tectonic caldera collapse (Fig. 13b). Thirdly, a new regional-tectonic strike-slip fault (Y-shear or PDZ) cut through and deactivated the pull-apart structure (Fig. 13c). A further evaluation of the role pull-apart structures may play in the caldera collapse phase at centres like Toba and Ranau, is thus possible from our experimental results.

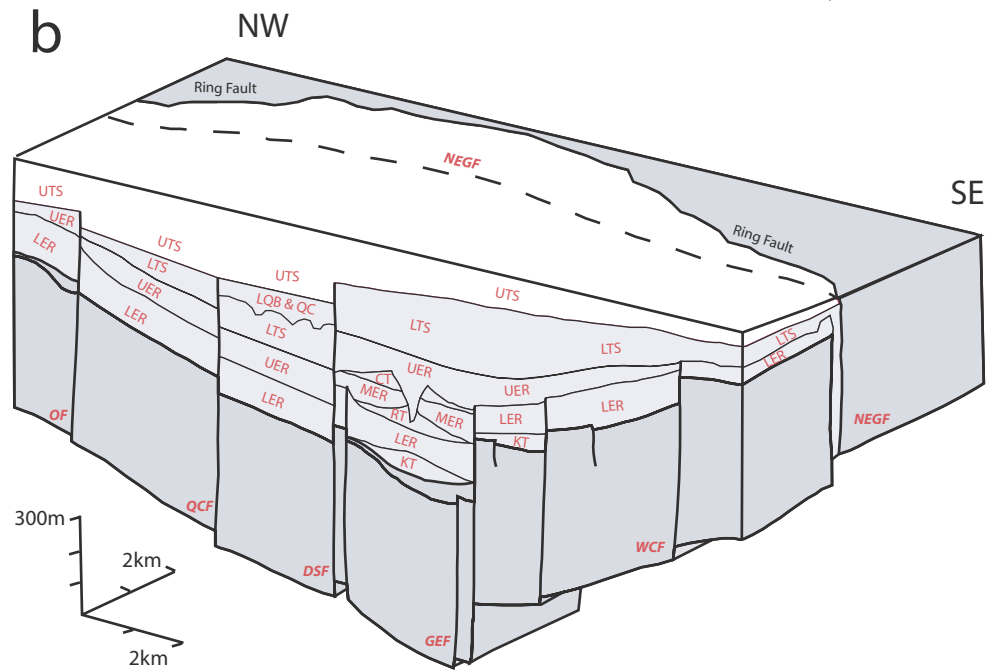
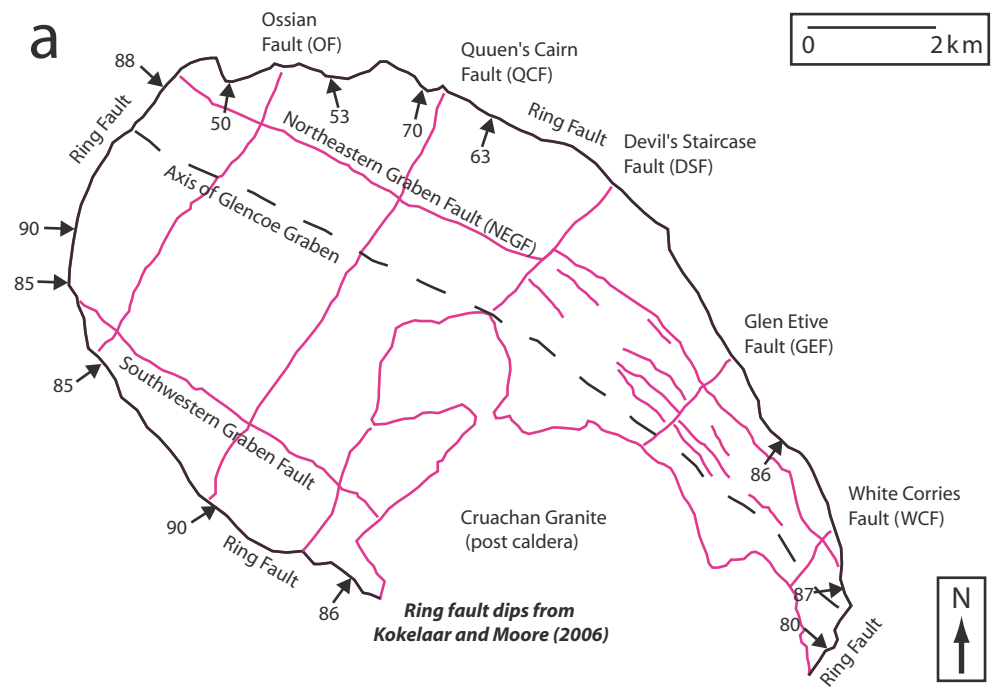
Firstly, though Bellier and Sebrier (1994) proposed that the pull-apart faults might entirely substitute for ring-faults during caldera collapse, our experiments suggest that this will occur only if the pull-apart faults entirely delimit or coincide with the magma chamber margins. Here, the pull-apart side-wall faults seem most likely to accommodate extension in the caldera periphery (Figs. 7b–d, 8a and 13c). Though they are likely to be buried in nature, subsidence controlling inner reverse ring-faults of purely volcano-tectonic origin may also form inside the side-wall faults (Figs. 7c, d, 8a, b and 13c). Secondly, though the exact timing between stages 2 and 3 is unclear in these natural examples (Fig. 13), our models show that where the Y-shear (or PDZ) cuts through the pull-apart and chamber prior to collapse, it can influence caldera development in the pull-apart by halting the propagation of subsidence controlling volcano-tectonic reverse faults (Figs. 7e, f, 8e, f and 13c).

Finally, regional strike-slip faults hosting rhyolite intrusions dissect the central floors of the Negra Muerta (NW Argentina—Riller et al. 2001; Ramelow et al. 2006) and Hopong calderas in a pattern very similar to the roof-dissecting Riedel shears and Y-shears in our models (Fig. 11b, c). These fault systems are therefore likely to be preferential pathways in nature for ascent of magma and other fluids before, during, or after caldera formation.

Summary and Conclusions

This study represents a first step in experimentally evaluating the role of strike-slip tectonics in caldera development

Fig. 12 a Outline map of intersecting regional structures within the polyhedral ring fault of Glencoe caldera (adapted from Moore and Kokelaar 1998). The main NW–SE trending Glencoe graben is cross-cut by several NE–SW trending regional tectonic faults, some of which bound subsidiary orthogonal grabens. Most faults now down-throw centrally. **b** Block diagram showing structure of floor and infill of Glencoe caldera, as restored to a plane horizontal surface presumed to have formed by eruption of the Upper Three Sisters (UTS) ignimbrite (adapted from Moore and Kokelaar 1998). The NW–SE line of section roughly coincides with the Glencoe Graben axis. The UTS possibly ponded against, but also extends beyond, the Northeast Graben Fault. UTS eruption is also inferred to have been associated with subsidence along the ring fault



- | | | | |
|-----|--------------------------------|-----|--|
| UTS | Upper Three Sisters Ignimbrite | CT | Crowberry Ridge Tuffs (Phreato-magmatic) |
| LQB | Lower Queen's Cairn Breccias | MER | Middle Etive Rhyolite |
| QC | Queen's Cairn Conglomerates | RT | Raven's Gully Tuffs (Phreato-magmatic) |
| LTS | Lower Three Sisters Ignimbrite | LER | Lower Etive Rhyolite |
| UER | Upper Etive Rhyolite | KT | Kingshouse Tuffs (Phreato-magmatic) |

that more detailed modelling and field analysis should complement. Our main findings are as follows:

1. Magma chamber geometry will exert the primary control on the geometry and development of subsi-

dence-controlling faults. At calderas forming above elliptical or elongate magma chambers, commonly found in strike-slip zones, reverse ring-faults should propagate from the short axis end of the chamber toward the long axis end. Since such 'ring' faults

comprised several linear segments, even in experiments without regional faults, a regional-tectonic control on linear ring-fault segments at natural calderas cannot be assumed.

- Regional fault reactivation during collapse can occur by structural grain exploitation and through fault-defined magma chamber margins. Where lying just inside and tangential to the magma chamber margins, regional strike-slip faults tend to reactivate to delimit the central caldera zone. Where lying just outside and tangential to the magma chamber margins, regional strike-slip faults tend to reactivate to delimit the peripheral caldera zone. Where defining ‘corners’ or

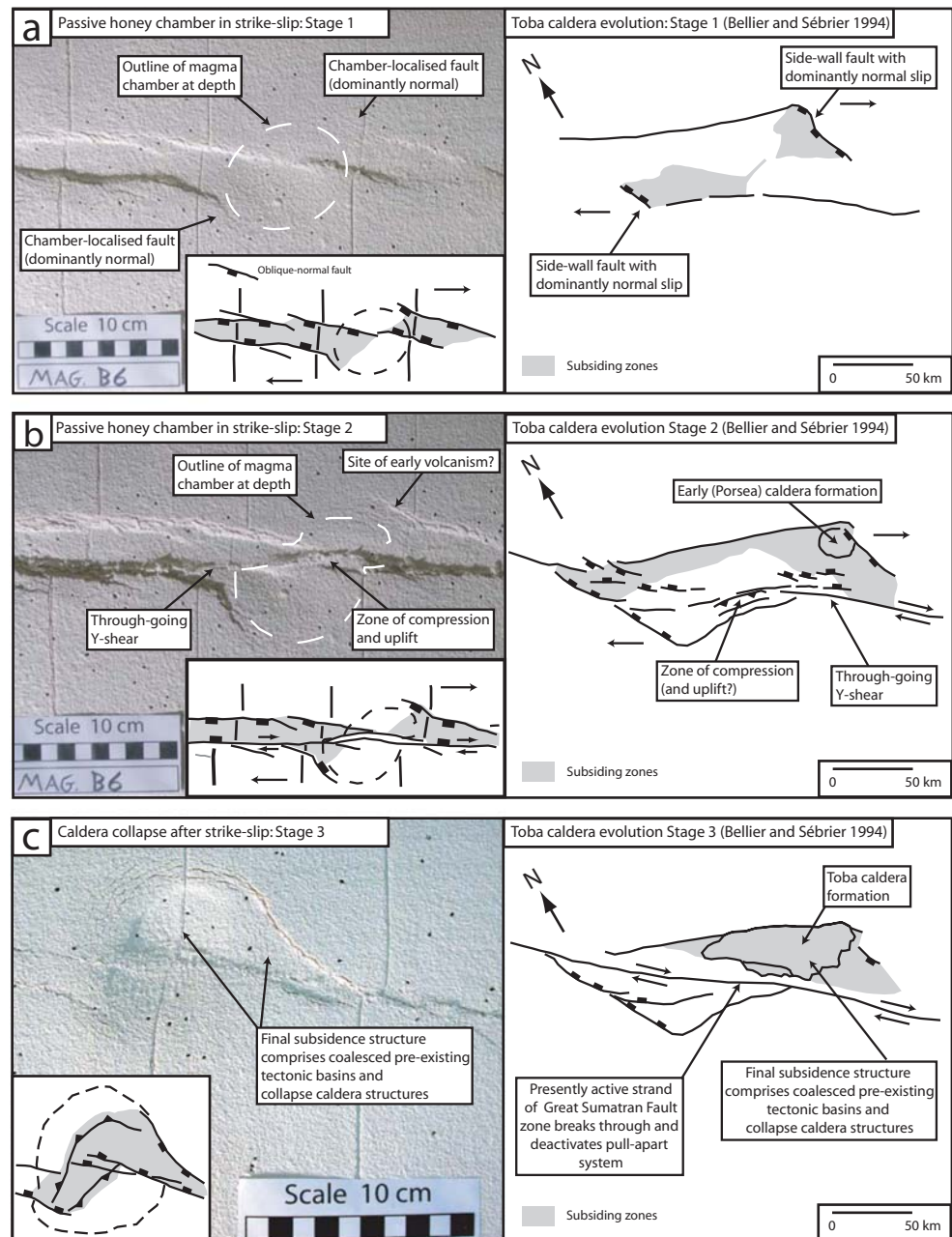
sharp bends in the chamber margin, regional-tectonic faults can also arrest the propagation of central zone reverse faults, and locally take up the volcano-tectonic displacement. The extent to which regional faults control caldera collapse may thus primarily depend on the extent to which they define or are coincident with the chamber margins.

- Long-lived, passive magma bodies or magmatic centres may localise marginal faults when subjected to regional transtension. These faults may result from rheological contrasts between the magmatic centre and the surrounding brittle crust, and are analogous to ‘side-wall’ faults of pull-apart graben.

Fig. 13 Tectonic evolutions of analogue models and of Toba caldera, Indonesia (redrawn from Bellier and Sébrier 1994).

a Both begin with pull-apart-like graben formation and subsidence, localised by the chamber in the model and by a releasing step-over in nature.

b Initial extension is followed by localised compression and formation of a through-going strike-slip fault, upon which all or most displacement is transferred. **c** Caldera subsidence and/or related peripheral extension are partly accommodated by reactivation of pre-existing structures. The relative timing of caldera formation and Y-shear breakthrough is unconstrained at Toba. In the model, Y-shear breakthrough occurred just prior to collapse and arrests propagating caldera reverse faults (Fig. 7 and 8)



4. Regardless of how a pull-apart basin localises, we infer that calderas formed in such structural settings will be strongly influenced by ‘side-wall’ faults. If linked with and tangential to the magma chamber margins, these faults will accommodate collapse-related extension in the peripheral caldera zone and act as peripheral zone bounding faults. They may also serve as sites for eruption. Note, however, that purely volcano-tectonic reverse faults may also occur within such pull-apart settings.
5. Dissection of the magma chamber roof by pre-collapse regional faults did not noticeably result in piecemeal collapse style in the central caldera zone, unlike as inferred at e.g. Glencoe caldera, Scotland. Direct comparison of single-collapse experiments to field studies of such multi-collapse calderas is difficult, however, and disparity may have three possible explanations. First, the low roof aspect ratios and flat magma chamber tops in our experiments may have promoted coherent central zone collapse. Second, the 10 to 100 m volcano-tectonic displacements along regional faults inferred at Glencoe would scale to <0.5 mm in the model, and thus may have been below our experimental ‘detection limit’. Third, the differential volcano-tectonic collapse of regional-fault-bound blocks at Glencoe may relate to spatially and temporally discrete, perhaps regional fault delimited, magma reservoirs.
6. Our experimental results highlight *pre-collapse* regional-tectonism as an important mechanism for generating a fragmented and differentially subsided caldera floor. Indeed, much of the differential displacement on regional faults at Glencoe caldera relates to background regional-tectonics rather than catastrophic volcano-tectonics. The experiments indicate that such differential pre-collapse floor displacements may be preserved by coherent to semi-coherent volcano-tectonic subsidence. This in turn highlights the need for demonstrable syn-collapse offset on a regional fault to accurately establish the extent to which an offset, or an ignimbrite thickness change, across the fault represents *volcano-tectonic* displacement.
7. The roof-dissecting strike-slip faults (R-shears and Y-shears) that cut the central zone in experiments may serve as pathways for magma ascent and eruption, as evidenced at several calderas in nature.

Acknowledgements We thank John Graham, Thomas Walter, Olivier Roche, and Tim Druitt for support, technical advice, and helpful discussion. An award to VRT and EPH from the Enterprise Ireland International Collaboration Programme greatly aided this work. EPH also appreciates financial assistance from the Department of Geology, the Graduate Studies Office and the Trinity Trust, Trinity College Dublin. Incisive and constructive reviews by G. Girard, U. Riller, O. Roche, and an anonymous reviewer helped us to significantly improve this paper.

References

- Acocella V, Salvini F, Funicello R, Faccenna C (1999) The role of transfer structures on volcanic activity at Campi Flegrei (Southern Italy). *J Volcanol Geotherm Res* 91:123–139
- Acocella V, Cifelli F, Funicello R (2000) Analogue models of collapse calderas and resurgent domes. *J Volcanol Geotherm Res* 104:81–96
- Acocella V, Korme T, Salvini F, Funicello R (2003) Elliptical calderas in the Ethiopian Rift: control of pre-existing structures. *J Volcanol Geotherm Res* 119:189–203
- Acocella V, Funicello R, Marotta E, Orsi G, de Vita S (2004) The role of extensional structures on experimental calderas and resurgence. *J Volcanol Geotherm Res* 129:199–217
- Aldiss DT, Ghazali SA (1984) The regional geology and evolution of the Toba volcano-tectonic depression, Indonesia. *J Geol Soc (Lond)* 141:487–500
- Basile C, Brun JP (1999) Transtensional faulting patterns ranging from pull-apart basins to transform continental margins: an experimental investigation. *J Struct Geol* 21:23–37
- Bellier O, Sebrier M (1994) Relationship between tectonism and volcanism along the Great Sumatran fault zone deduced by SPOT image analyses. *Tectonophysics* 233:215–231
- Bellier O, Bellon H, Sébrier M, Sutanto, Maury RC (1999) K-Ar age of the Ranau Tuffs: implications for the Ranau caldera emplacement and slip-partitioning in Sumatra (Indonesia). *Tectonophysics* 312:347–359
- Benn K, Odone F, de Saint Blanquat M (1998) Pluton emplacement during transpression in brittle crust; new views from analogue experiments. *Geology* 26:1079–1082
- Bosworth W, Burke K, Strecker M (2003) Effect of stress fields on magma chamber stability and the formation of collapse calderas. *Tectonics* 22:1042
- Branney MJ (1995) Downsag and extension at calderas: new perspectives on collapse geometries from ice-melt, mining, and volcanic subsidence. *Bull Volcanol* 57:303–318
- Branney MJ, Kokelaar P (1994) Volcanotectonic faulting, soft-state deformation, and rheomorphism of tuffs during development of a piecemeal caldera, English Lake District. *Geol Soc Amer Bull* 106:507–530
- Carr WJ, Quinlivan WD (1968) Structure of Timber Mountain resurgent dome, Nevada Test Site. *Mem Geol Soc Amer* 110:99–108
- Chesner CA (1998) Petrogenesis of the Toba Tuffs, Sumatra, Indonesia. *J Petrol* 39:397–438
- Cole JW, Milner DM, Spinks KD (2005) Calderas and caldera structures: a review. *Earth-Sci Rev* 69:1–26
- Corti G, Moratti G, Sani F (2005) Relations between surface faulting and granite intrusions in analogue models of strike-slip deformation. *J Struct Geol* 27:1547–1562
- Cruden AR (1998) On the emplacement of tabular granites. *J Geol Soc (Lond)* 155:853–862
- Dingwell DB (1999) Granitic melt viscosities. *Geol Soc Lond Spec Publ* 168:27–38
- Donnadieu F, Merle O (1998) Experiments on the indentation process during cryptodome intrusions; new insights into Mount St. Helens deformation. *Geology* 26:79–82
- Dooley T, McClay K (1997) Analog modeling of pull-apart basins. *Bull Am Assoc Pet Geol* 81:1804–1826
- Druitt TH, Sparks RSJ (1984) On the formation of calderas during ignimbrite eruptions. *Nature* 310:679–681
- Girard G, van Wyk de Vries B (2005) The Managua Graben and Las Sierras-Masaya volcanic complex (Nicaragua); pull-apart localisation by an intrusive complex: results from analogue modelling. *J Volcanol Geotherm Res* 144:37–57

- Goff F, Gardner JN (1994) Evolution of a mineralized geothermal system, Valles Caldera, New Mexico. *Econ Geol* 89:1803–1832
- Goodman RE (1989) Introduction to rock mechanics. Wiley, New York
- Hickman RG, Dobson PF, van Gerven M, Sagala BD, Gunderson RP (2004) Tectonic and stratigraphic evolution of the Sarulla graben geothermal area, North Sumatra, Indonesia. *J Asian Earth Sci* 23:435–448
- Hildreth W, Mahood GA (1986) Ring-fracture eruption of the Bishop Tuff. *Geol Soc Amer Bull* 97:396–403
- Holohan EP, Troll VR, Walter TR, Münn S, McDonnell S, Shipton ZK (2005) Elliptical calderas in active tectonic settings: an experimental approach. *J Volcanol Geotherm Res* 144:119–136
- Hubbert MK (1951) Mechanical basis for certain familiar geologic structures. *Geol Soc Amer Bull* 62:355–372
- Hutton DHW, Reavy RJ (1992) Strike-slip tectonics and granite petrogenesis. *Tectonics* 11:960–967
- Jacques JM, Reavy RJ (1994) Caledonian plutonism and major lineaments in the SW Scottish Highlands. *J Geol Soc (Lond)* 151:955–969
- Jellinek AM, DePaolo DJ (2003) A model for the origin of large silicic magma chambers: precursors of caldera-forming eruptions. *Bull Volcanol* 65:363–381
- John DA (1995) Tilted middle Tertiary ash-flow calderas and subjacent granitic plutons, southern Stillwater Range, Nevada; cross sections of an Oligocene igneous center. *Geol Soc Amer Bull* 107:180–200
- Kennedy B, Stix J, Vallance JW, Lavallée Y, Longpré M-A (2004) Controls on caldera structure: results from analogue sandbox modeling. *Geol Soc Amer Bull* 116:515–524
- Kokelaar P, Moore I (2006) Classical areas of British geology: Glencoe caldera volcano, Scotland. British Geological Survey memoir. British Geological Survey, Keyworth
- Komuro H (1987) Experiments on cauldron formation: a polygonal cauldron and ring fractures. *J Volcanol Geotherm Res* 31:139–149
- Lipman PW (1997) Subsidence of ash-flow calderas; relation to caldera size and magma-chamber geometry. *Bull Volcanol* 59:198–218
- Marti J, Ablay GJ, Redshaw LT, Sparks RSJ (1994) Experimental studies of collapse calderas. *J Geol Soc (Lond)* 151:919–929
- Molyneux SJ, Hutton DHW (2000) Evidence for significant granite space creation by the ballooning mechanism; the example of the Ardara Pluton, Ireland. *Geol Soc Amer Bull* 112:1543–1558
- Moore I, Kokelaar P (1998) Tectonically controlled piecemeal caldera collapse; a case study of Glencoe Volcano, Scotland. *Geol Soc Amer Bull* 110:1448–1466
- Nappi G, Renzulli A, Santi P (1991) Evidence of incremental growth in the Vulsinian calderas (central Italy). *J Volcanol Geotherm Res* 47:13–31
- Orsi G, De Vita S, Di Vito M (1996) The restless, resurgent Campi Flegrei nested caldera (Italy): constraints on its evolution and configuration. *J Volcanol Geotherm Res* 74:179–214
- Ramelow J, Riller U, Romer R, Oncken O (2006) Kinematic link between episodic trapdoor collapse of the Negra Muerta caldera and motion on the Olacapato-El Toro fault Zone, southern central Andes. *Int J Earth Sci* 95:529–541
- Rampino MR, Self S (1992) Volcanic winter and accelerated glaciation following the Toba super-eruption. *Nature* 359:50–52
- Riller U, Petrinovic I, Ramelow J, Strecker MR, Oncken O (2001) Late Cenozoic tectonism, collapse caldera and plateau formation in the Central Andes. *Earth Planet Sci Lett* 188:299–311
- Roche O, Druitt TH, Merle O (2000) Experimental study of caldera formation. *J Geophys Res* 105:395–416
- Roman-Berdiel T (1999) Geometry of granite emplacement in the upper crust; contributions of analogue modelling. *Geol Soc Lond Spec Pub* 168:77–94
- Scaillet B, Holtz F, Pichavant M (1997) Rheological properties of granitic magmas in their crystallization range. In: Bouchez JL, Hutton DHW, Stephens WE (eds) Granite: from segregation of melt to emplacement fabrics. Kluwer, Dordrecht, pp 11–29
- Schellart WP (2000) Shear test results for cohesion and friction coefficients for different granular materials; scaling implications for their usage in analogue modelling. *Tectonophysics* 324:1–16
- Schöpfer MPJ, Steyrer HP (2001) Experimental modeling of strike-slip faults and the self-similar behaviour. *Geol Soc Am Mem* 193:21–27
- Schultz RA (1996) Relative scale and the strength and deformability of rock masses. *J Struct Geol* 18:1139–1149
- Self S, Rampino MR, Newton MS, Wolff JA (1984) Volcanological study of the great Tambora eruption of 1815. *Geology* 12:659–663
- Skilling IP (1993) Incremental caldera collapse of Suswa volcano, Gregory Rift Valley, Kenya. *J Geol Soc (Lond)* 150:885–896
- Smith RL, Bailey RA (1968) Resurgent cauldrons. *Geol Soc Am Mem* 116:613–662
- Spinks KD, Acocella V, Cole JW, Bassett KN (2005) Structural control of volcanism and caldera development in the transtensional Taupo Volcanic Zone, New Zealand. *J Volcanol Geotherm Res* 144:7–22
- Troll VR, Walter TR, Schminke H-U (2002) Cyclic caldera collapse: Piston or piecemeal subsidence? Field and experimental evidence. *Geology* 30:135–138
- Ventura G, Vilardo G, Milano G, Pino NA (1999) Relationships among crustal structure, volcanism and strike-slip tectonics in the Lipari-Vulcano volcanic complex (Aeolian Islands, southern Tyrrhenian Sea, Italy). *Phys Earth Planet Inter* 116:31–52
- Walter TR, Troll VR (2001) Formation of caldera periphery faults: an experimental study. *Bull Volcanol* 63:191–203
- Woodcock NH, Schubert C (1994) Continental strike-slip tectonics. In: Hancock PL (ed) Continental deformation. Pergamon, Oxford, pp 251–263